Remote wide angle view broad wavelength viewing system compatible with D-T operations in JET

I. Balboa[1], E. Rose[1], G. F. Matthews[1], D. Croft[1], M. Stamp[1], S. A. Silburn[1], J. C. Williams[1], D. Hepple[1], A. Huber[2], S. Whetham[1], D. Iglesias[1,9], D. J. Kinna[1], M. Beldishevski[1], J. Figueiredo[3,4], C. Perez Von Thun[2,10], G. Jones[1], N. Balshaw[1], L. D. Horton[5,6], R. C. Lobel[1], I. J. Pearson[1], K. W. Pepperell[1], G. Fishpool[1], B. Lane[1], K-D. Zastrow[1], G. Arnoux[1], G. Bodnar[7], P. Carman[1], P. Carvalho[1,3], N. J. Conway[1], N. Gupta[1], V. Huber[2], G. Kocsis[7], A. Manzanares[8], P. Puglia[1,6], C. Ruiz de Galarreta[8], C. Marren[1], R. Otín[1], J. Naish[1], V. K. Thompson[1] and the JET Contributors[11]

[1] United Kingdom Atomic Energy Authority, Culham Science Centre, Abingdon, Oxon OX14 3DB, United Kingdom of Great Britain and Northern Ireland
[2] Forschungszentrum Jülich GmbH, Institut für Energie und Klimaforschung, Plasmaphysik 52425, Jülich, Germany
[3] Instituto de Plasma e Fusão Nuclear, Instituto Superior Técnico, Universidad de Lisboa 1049-001 Lisboa, Portugal
[4] EUROfusion Programme Management Unit, Boltzmannstr. 2, 85748 Garching, Germany
[5] EUROfusion Programme Management Unit, Culham Science Centre, Culham OX14 3DB, United Kingdom of Great Britain and Northern Ireland
[6] Ecole Polytechnique Fédérale de Lausanne (EFPL), Swiss Plasma Center (SPC), CH-1015 Lausanne, Switzerland
[7] Centre for Energy Research, POB 49, H-1525, Budapest, Hungary
[8] Laboratorio Nacional de Fusión, CIEMAT, Madrid, Spain
[9] Currently at ITER Organization, Route de Vinon-sur-Verdon, CS90 046, 13067 Saint Paul Lez Durance Cedex, France
[10] Currently at Institute of Plasma Physics and Laser Microfusion, Hery 23, 01-497 Warsaw, Poland
[11] See the author list of 'Overview of JET results for optimising ITER operation' by J. Mailloux *et al*. 2022 *Nuclear Fusion* **62** 042026'

E-mail: Itziar.Balboa@ukaea.uk

Received xxxxxx
Accepted for publication xxxxxx
Published xxxxxx

Abstract

Imaging diagnostics in Joint European Torus have become essential in the study of plasma wall interactions and the protection of the plasma facing components. During deuterium operations, the location of these diagnostics was at close proximity to the vessel. However, for the 50-50 deuterium-tritium operation, the neutron yield impact onto the electronics of these imaging diagnostics would have caused them to fail completely at these locations. Shielding these systems from neutrons is achieved by relocating a selected number of these imaging systems to outside the Torus Hall (*i.e.* to the other side of the biological shield wall). The relocation encompasses the construction of two new lines of sight crossing through the biological shield wall and each of them using an optical relay which extends to separate ports in the machine.
This article starts with a brief description of two new viewing systems. However, it focuses on the optical modelling and engineering design of one of them which is a multiple camera system producing a wide angle view (WAV) of the inside of the vessel. This WAV system

has been used successfully during the recent D-T campaign. It operates in a broadband wavelength range extending from the visible to the middle infrared. It also incorporates a novel in-house horizontal kinematic mirror mount made from glass reinforced plastic as part of the optical relay. The operational stability of the WAV system has also been assessed and some post design improvements implemented.

Keywords: remote, camera, broadband, mirror mounting, JET

1. Introduction

One of the main diagnostic capabilities of the Joint European Torus (JET) are camera systems because they are used in a number of applications such as the measurement of temperature and heat fluxes on the plasma facing components, characterisation of different plasma events such as edge localised modes (ELMs) and monitoring of impurities (see [1]-[10]). The cameras are also a crucial and integral part of JET first wall protection system (see [1] and [9]). In preparation for the JET deuterium-tritium (D-T) campaign, a work package of diagnostic enhancements was funded by EUROfusion and JET Operating Contract (JOC) (see [11]) to ensure that the operation of a selected number of diagnostics would be compatible with the D-T operation. Among them, there was the installation of camera diagnostics with different fields of view. Operation of JET with 50-50 D-T plasmas and high auxiliary heating power generates sufficient neutron dose to cause irreversible damage to any camera diagnostics within the biological shield wall after just one plasma pulse. Therefore, it was necessary to identify the most effective way to shield the camera systems from the neutrons while maintaining sufficient viewing coverage of the plasma facing components. The solution presented here describes the installation of a wide-angle view (WAV) diagnostic system comprising a mirror relay adapted to an existing endoscope in combination with multiple camera systems located outside the Torus Hall (TH) providing several new diagnostic views of the machine with different wavelength ranges and functional applications. A further paper will be focusing on a second diagnostic system which was dedicated to viewing the divertor using a separate line of sight (LOS).

New camera labs were built to provide housing for all the diagnostic viewing systems. The new labs extend across three floors on the outside of one of the sides of the biological shield wall. In addition, new penetrations were drilled through the biological shield wall in order to provide the two separate lines of sight.

This paper focuses on the description of the WAV relay and diagnostic systems, in particular its optical and mechanical design as well as its operational performance.

Overviews of the endoscope field of view and the optical relay line of sight are presented in sections 2 and 3 respectively. Details of the instrumentation for each of the diagnostic camera systems are presented in section 4. A detailed summary of the mirror relay optical modelling is presented in section 5 and the engineering analysis of the mechanical mounts and support structures in the TH, paying attention to stresses, deformations and stability due to self-weight and magnetic induced loads, is presented in section 6. The optics and mechanical installations outside the TH are presented in section 7 and the penetration in the biological shield wall is discussed in section 8. Radiation shielding is described in section 9 and a summary of operational experience is presented in section 10.

2. Field of View

The WAV target field of view is required to include a number of plasma-facing components to enable monitoring and protection of the machine. A 3D model view of the target field of view with the main tiles labelled is provided in Figure 1. This includes the inner wall guard limiter (IWGL), narrow poloidal limiter (NPL), upper dump plate tiles (UDPT), Upper Inner Wall Protection tile (UIWP); antenna systems such as Ion Cyclotron Resonance Heating (ICRH), Lower Hybrid (LH) and ITER-like Antenna (ILA), as well the re-ionisation tiles denoted as REION4 and BEION4 in octant 4 and the divertor region (Div). The two-character term shown in the figure (e.g. ‘4D’, ‘3B’) represents the identification number of the specific inner or outer guard limiter. The fourth-character term identifies the specific tile within the respective guard limiter. ‘RFB’ represents the name of the specific ICRH antenna system included in this target view and ‘sep’ corresponds to the ‘septum’, which is the limiter that divides the ICRH antenna in two halves.

The WAV field of view represents a poloidal cross section of the machine using the view originating from octant 5 looking clockwise around some of the sectors (octants) of the inside of the machine vessel.

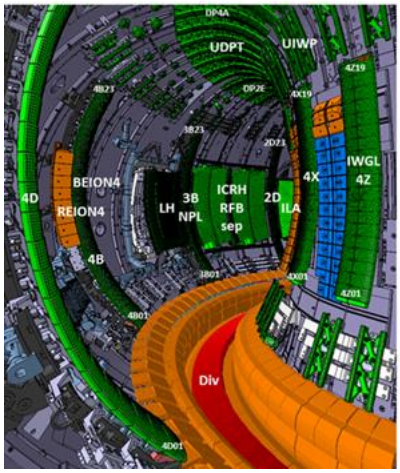

Figure 1 3D model view showing the target field of view for the WAV LOS (see text for the meaning of the different acronyms).

3. Line of Sight

A picture of JET is given in Figure 2 which presents the JET tokamak and the transformer limb surrounding the tokamak (see [12]). Therefore, there is a transformer limb around each octant or sector.

The target field of view shown above is produced using the WAV line of sight depicted in Figure 3. The total optical path length of the WAV LOS is 40 m. The bottom right hand side of Figure 3 presents a poloidal section of the inside of the machine vessel. Next to it, there is one end of the endoscope inside the vessel which is then connecting the light path towards two mirror assemblies mounted onto the transformer limb.

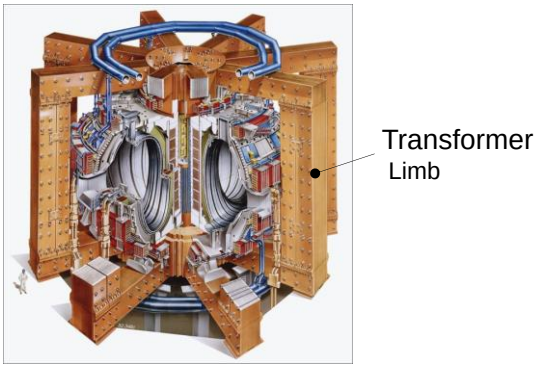

Figure 2 Picture showing JET tokamak

The LOS extends through the biological shield wall into purpose built labs in the adjacent building (J1F) to the west side of the Torus Hall (TH). The mirror relay consists of four mechanically supporting mirror assemblies which are known as 'M1&M3', 'M2&M4', 'M5' and 'M6'. The mirror assemblies are named after the sequence of reflections from each mirror (see Figure 3). The first two mirror assemblies are located inside the Torus Hall whereas 'M5' and 'M6' are in the second (or 'Middle') J1F lab. Note that the section in Figure 3 showing the components outside the TH spans two labs, the lower and middle. The mid-infrared camera system is in the lower lab and all other camera systems are located in the level above in the 'Middle' lab.

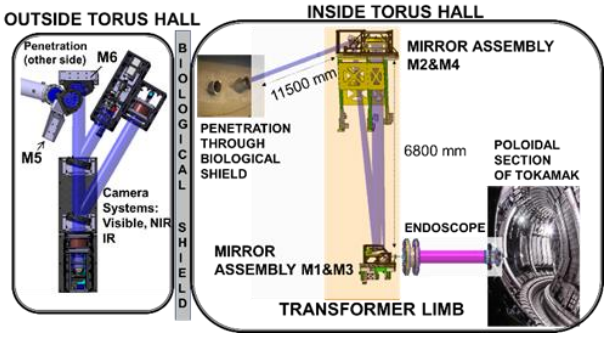

Figure 3 Schematic of WAV line of sight. The light path starts from the bottom right hand corner (poloidal section of the tokamak) and it ends on the left hand side of the figure (i.e.outside of the Torus Hall).

The selection of this line of sight was based on three reasons: first, the re-utilization of the same endoscope that was used for the protection camera systems installed in the Torus Hall prior to the construction of this line of sight. Secondly, having sufficient space available for the construction of suitable labs to house all the camera systems corresponding to this line of sight and finally, the fact that the same octant of the tokamak (which was octant 5) was also the best location for the second line of sight dedicated to imaging the divertor region (DIR).

4. Systems Specifications

The WAV diagnostic system comprises a total of five camera systems. The key requirements were to reproduce the field of view of the existing systems (*i.e.* the ones that needed to be relocated prior to the construction of this line of sight). This also meant to be able to reproduce the spatial and temporal resolutions. For the camera systems operating in the near and mid-infrared, an additional requirement was to achieve the same temperature range. Each individual camera provides a different functionality. Table 1 lists all the camera systems using the WAV line of sight. The camera systems cover visible, near infrared and middle infrared wavelength ranges which are defined as 400-700 nm, 0.9-1.2 μm and 3.0-3.6 μm respectively. However, the delivered performance of the optics extended the near infrared range to 1.3 μm (see Figure 15 and Figure 16). It should be pointed out that all the images presented in this section associated with JET pulses were obtained using a software tool called JUVIL (see [13]).

Camera System ID & Application for the WAV viewing system	**Wavelength range**

KLDT-P5WA: Protection of plasma facing components by measuring surface temperature	Near infrared
KLDT-O5WB: Display plasma pulse	Visible
KLDT-E5WC: In-vessel tiles temperatures & heat fluxes	Mid-Infrared
KLDT-E5WD: Monitoring of Impurities	Visible
KLDT-E5WE: High-speed plasma imaging	Visible

Table 1 WAV camera systems and their applications.

The criterion for determining the working wavelength is based on the required temperature range and the dependence with tungsten emissivity. Tungsten emissivity has a very weak dependence with temperature at the near infrared wavelength of ~1.2 μm (see [1]). This makes the near infrared wavelength range suitable for protection of the plasma facing components. Secondly, in terms of the measuring temperature range, the mid-infrared wavelength range enables the measurement of lower temperatures in comparison with the near infrared wavelength range as predicted by Planck's law. Specifically for the WAV system, this is very advantageous for scientific applications. Using the mid-infrared wavelength range, the minimum surface temperature can go as low as 300°C as demonstrated in reference [14]. On the other hand, using the near infrared wavelength range, the minimum temperature is ~600ºC which is not a problem in itself for the protection cameras, since the main requirement is to measure accurately temperatures above the 900º C. This is why the near infrared wavelength range is used for protection and the mid-infrared wavelength range is used for scientific applications.

The specifications of the different camera systems of WAV are presented in two tables. Table 2 reports the specifications of the three cameras operating in the visible range. On the other hand, Table 3 lists the key parameters for the near infrared camera (KLDT-P5WA) used for protection and the mid-infrared scientific camera (KLDT-E5WC) used for the measurement of temperature and heat fluxes on the plasma facing components. It should be pointed out that a number of spectral line filters for Beryllium, Neon, Helium and Deuterium are used for the spectroscopy and high speed camera as listed below.

Specifications	**KLDT-O5WB Operations**	**KLDT-E5WD Spectroscopy**	**KLDT-E5WE High Speed**
Pixel size (μm)	5.86	16	17
Sensor Size	11.3 × 7.1 mm	512 × 512 pixels 8.2 × 8.2 mm	1024 × 1024 pixels 17.4 × 17.4 mm
Sensor Type	CMOS	CCD (EMCCD)	CMOS
Exposure	32 μs - 1000 s	2 μs - 40 s	1 μs – 20ms
Frame Rate	25Hz	67 fps (FF) – 3000 fps	50 fps-3 kfps
Digitisation	8 bits	16 bits	10 bits
Interface	USB 3.0	FireWire	FireWire
Optical Filter	n/a	BeII, Dβ, Dα, BeI	Ne I, He I, Dα
Dimensions (mm)	78 × 84	114.3 × 120.65 × 17.78	212.6 × 131.4 × 289.2
Weight (kg)	0.41	2.8	4.9
Model	ASI174MC	Evolve 512 Delta	Fastcam APX-RS
Supplier	ZWO	Photometrics	Photron

Table 2 Specifications of the WAV visible cluster. (FF: Full Frame).

The operational camera (KLDT-O5WB) does not require a filter since it is used for display purposes. Figure 4 displays two images produced by the operational camera. The image on the left was obtained using in-vessel illumination. This is the reason for the bright series of spots near the top of the left image of Figure 4 image. The image on the right of Figure 4 represents a single frame obtained for pulse 92735 at 55.109 s. This camera is used in the control room by the experimental team to view the plasma in real time.

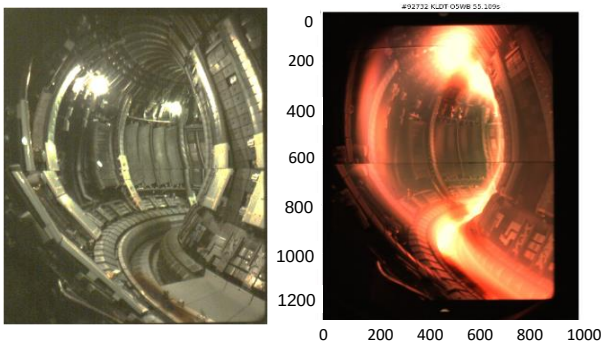

Figure 4 Images produced by the operational camera KLDT-O5WB. Left: in-vessel image taken during shutdown in 2016. Right: Image frame from pulse 92735. Horizontal and vertical axes are pixel units.

It should be pointed out that with the exception of the spectroscopy camera, the sensor type is complimentary metal oxide semiconductor (CMOS), the reason being that it is more versatile for those applications requiring selecting a region of interest within the sensor. However, the spectroscopy camera (KLDT-E5WD) was chosen as an electron multiplying CCD (EMCCD) because of the requirement for high sensitivity. Figure 5 shows two images of the spectroscopy camera (KLDT-E5WD). The image on the left was taken during shutdown using in-vessel illumination with no filter in use. The bright stripes across the image are there due to the large integration time of (several seconds) and blurring effect which is typical of CCD sensors when parts of the image saturate as it is the case here. The image on the right was produced during

pulse 98300 at 49.025 s. The horizontal and vertical axes have pixel units and represent the area of the sensor used for the image. The colour map is showing the raw data in 'counts' and the numbers represent the intensity levels. Since the filter used was Dα, the image shows the level of Deuterium emission as a function of colour gradient.

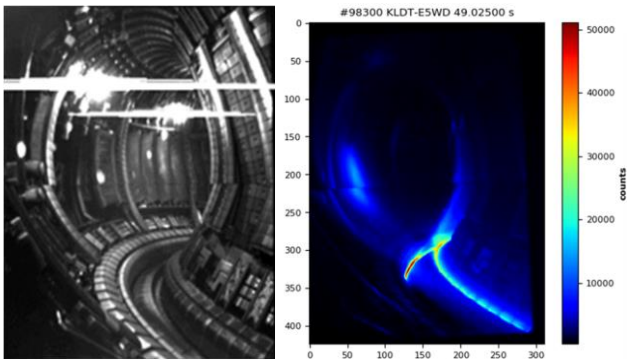

Figure 5 Two images produced with the spectroscopy camera (KLDT-E5WC). Left: In-vessel image taken during shutdown period and using in-vessel illumination. Right: Image taken from pulse 98300 at 49.025 s.

The third camera in the visible cluster is the high speed camera (KLDT-E5WE) used for the monitoring of fast events within the plasma. The image on the left of Figure 6 is taken without a filter and it was obtained during the shutdown period. The exposure time was set to several seconds and thus saturating in those points corresponding to the in-vessel illumination system. On the other hand, the image on the right of Figure 6 was taken during pulse 95132 and it clearly captures plasma structures during the pulse.

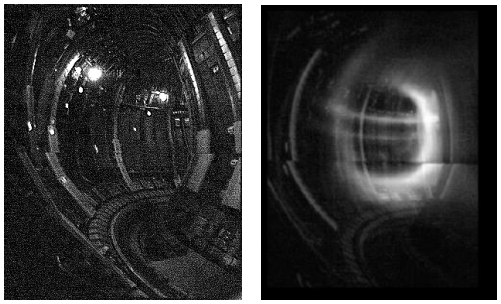

Figure 6 Two images obtained with the high-speed camera. Left: In-vessel image taken during shutdown using in-vessel illumination. Right: Image produced during pulse 95132 at 48.468501 s.

The websites for the suppliers listed are as follows: ZWO (https://astronomy-imaging-camera.com/), Photometrics (http://www.photometrics.com/) and Photron (https://photron.com/).

The specifications for the near and middle infrared cameras are listed in Table 3. Both types used CMOS sensors. The websites of the suppliers are listed as follows: New Imaging Technologies (https://new-imaging-technologies.com) and FLIR (https://www.flir.co.uk).

Specifications	**KLDT-P5WA Protection**	**KLDT-E5WC Mid-Infrared scientific camera**
Pixel size (μm)	15	30
Sensor Size	640 × 512 pixels 9.6 × 7.68 mm	320 × 256 pixels 9.6 × 7.68 mm
Sensor Type	InGaAs Monochrome CMOS	CMOS InSb focal plane array
Exposure	100 μs – 25 ms	1 μs – 20 ms
Frame Rate	25 Hz standard (Range: 25-150 Hz)	380 Hz
Digitisation	14 bits	14 bits
Interface	USB 2.0	Giga Ethernet
Optical Filter	1.250 ± 0.25 μm	3.25 ± 0.25μm
Dimensions (mm)	64 × 56.3 × 47.1	230 × 110 × 150
Weight (kg)	≲ 0.23	~ 3
Wavelength Range (μm)	0.9-1.7	1.5-5.1
Model	WiDy SWIR 640U-ST	Titanium 550 (customised model)
Supplier	New Imaging Technologies (NIT)	FLIR

Table 3 Specification for the near-infrared protection camera and the Mid-infrared scientific camera (KLDT-P5WA and KLDT-E5WC respectively).

Figure 7 displays an image of the protection camera KLDT-P5WA during pulse 92733 at 55.430 s. This image was taken during a disruption. In general, disruptions provide such a high level of plasma light that it is possible to obtain an image from KLDT-P5WA of the inside of the vessel (at the expense of saturating the detector as is the case along the central column, in the inner side of the vessel). Disruptions are the best option to confirm the alignment and focusing of the protection cameras because of their operation in relatively narrow wavelength bands of the near infrared. The horizontal and vertical axis are in pixel units and the grey scale represents the light intensity in 'counts' with arbitrary units (see Table 3 for the filter specification).

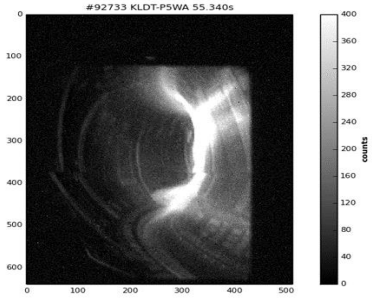

Figure 7 Image of the protection camera (KLDT-P5WA) for pulse 92733 at time 55.340 s.

The mid-infrared wide angle view camera (KLDT-E5WC) is only used for the measurement of temperatures (see [15]) due to its low spatial resolution (see also section 7.2). Figure 8 shows on the left-hand side an image of the vessel taken during baking phase before resuming operations. On the right-hand side, it shows an image obtained during pulse 93435 at 52.15 s. The colour map illustrates the different intensity levels which are translated into temperature during the processing of the raw data. As an additional note, the operational temperature range for this camera starts extends from 300 °C up to 1700 °C.

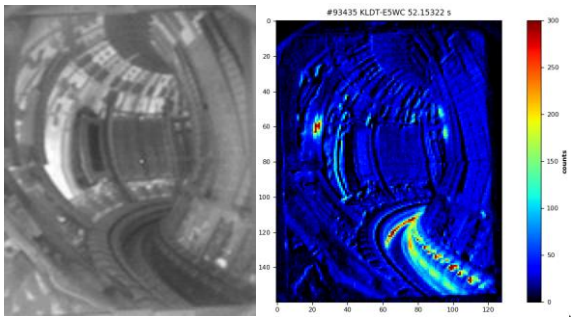

Figure 8 Left: Image obtained from mid-infrared KLDT-E5WC during vessel baking. Right: Image frame from pulse 93435.

5. Optical Modelling

The aim of the optical design is to be able to reproduce the optical performance of the diagnostics that have been relocated. However, given the fact that additional components are required in order to relay the light to outside the TH, it is clear that it will not be possible to obtain the same optical transmittance for the entire system compared with when the diagnostics were inside the TH. Thus, the main requirement for the new systems located outside the TH is to achieve the same field of view dimensions as to when they were inside the TH and to be able to distinguish the same plasma facing components. The material selection for the optical components was based on their suitability for the specific operational wavelength range and their reliability and resilience in fusion environments. It is important to point out that the complete optical design includes components integrated to the machine as well as the new components that have been installed to relay the light to the new systems located outside the TH. The optical design was carried out using Zemax (https://www.zemax.com). The required manufacturing tolerances were also calculated using Zemax. The criterion used for the calculation of the critical parameters was the RMS Spot Radius in millimetres (with 1000 Monte Carlo cycles). The existing components are the ones already integrated to the machine: in-vessel pair of collection mirrors, pair of fold mirrors and endoscope steering mirror, and a double set of fused silica windows.

The new components comprise six mirrors in total, two custom dichroic optics, plus the optical lenses and filters attached to each of the camera systems. The specifications and performance for each of the optical lenses attached to each camera respectively will be described separately. Figure 9 shows a schematic of all the elements of the WAV line of sight. For better visualisation, this figure needs to be compared with Figure 3. In Figure 9, starting with position ‘A’, this represents the in-vessel mirrors and ‘B’ denotes mirror M1, which is the first mirror in the mirror relay. Although it is not shown in the figure, the location of the KL14 endoscope is between ‘A’ and ‘B’ together with the double set of vacuum windows close to ‘B’. ‘C’, ‘D’ and ‘E’ corresponds to mirrors M2, M3 and M4 respectively of the mirror relay within the TH. Then ‘F’ and ‘G’ show the positions of mirrors M5 and M6 of the relay; these two positions are located outside the TH and inside one of the camera labs (see Figure 3). This completes the mirror relay. Thus, ‘H’ and ‘J’ refer to two dichroic optics which transmit the middle Infrared wavelength camera light (KLDT-E5WC) and separate light for the visible cameras (KLDT-O5WB, KLDT-E5WD and KLDT-E5WE) and near infrared camera (KLDT-P5WA) respectively. All these cameras are shown on the same plane. The middle infrared camera (KLDT-E5WC) denoted as ‘K’ occupies the camera lab below the level of the other four cameras located at positions ‘L’ (visible cluster) and ‘M’ (near infrared).

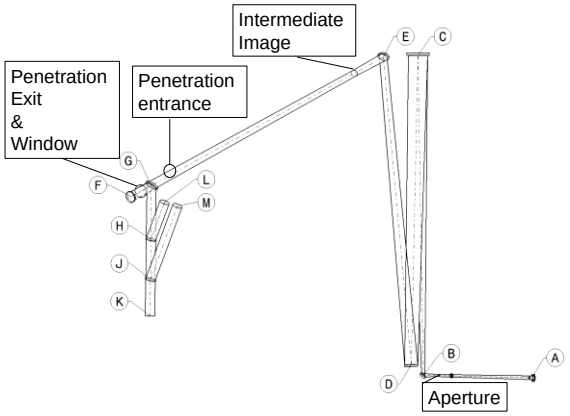

Figure 9 Main components in WAV line of sight. A: in-vessel mirrors, B: mirror (M1), C: mirror (M2), D: mirror (M3), E: mirror (M4), F: mirror (M5), G: mirror (M6), H: First Dichroic (D1), J: Second Dichroic (D2), K: KLDT-E5WC, L: Three camera systems (KLDT-O5WB, KLDT-E5WD, KLDT-E5WE), M: KLDT-P5WA.

This section has been subdivided into 5 sub-sections to explain in more detail the modelling of the main components.

5.1 In-vessel mirrors and KL14 endoscope

As per Figure 3 and Figure 10, the in-vessel mirrors box and the KL14 endoscope (see references [1] and [16]) form the existing optics which have been re-used for the new WAV line of sight.

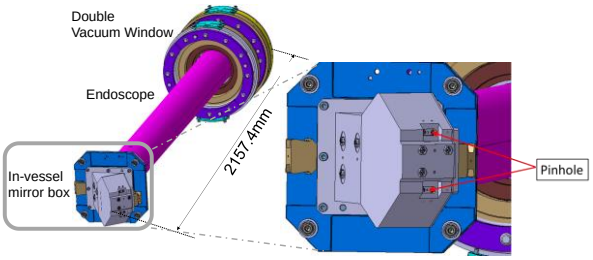

Figure 10 Front view of the in-vessel mirrors box and KL14 endoscope with zoom on the in-vessel mirror box.

A picture showing the different elements of the in-vessel mirrors box is provided in Figure 11. There are two pinholes top and bottom as well as two parabolic mirrors and two-fold mirrors. The fold mirrors direct the light towards the flat steering mirror which in turn reflects the light along the endoscope (see [17]). The rectangular plane mirror is inside the KL14 endoscope. However, the two sets of parabolic and fold mirrors making up the mirror box are located inside the vessel attached to a 'plug' inserted in the end of one of the vacuum vessel 'Limiter Guide Tubes'.

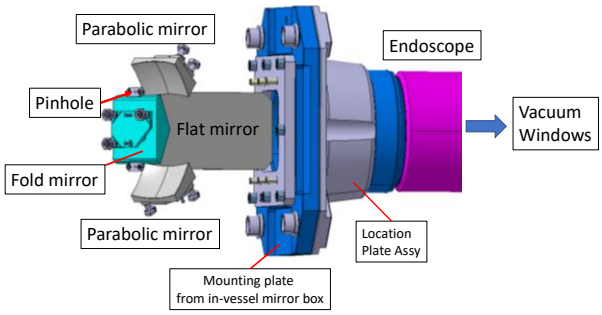

Figure 11 Components from in-vessel mirror box.

The purpose of having two mirror sets is to produce a top and bottom view of the vessel in the combined image. For each view, there is one optical model. Figure 12 shows in more detail the front and back ends of the endoscope for the top view only.

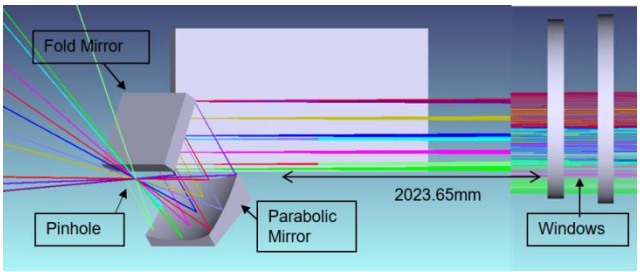

Figure 12 Ray tracing of the top view of the KL14 endoscope.

Table 4 shows a description of the optical components inside the endoscope. The parabolic mirrors have a conic constant of -1.00 which is not shown in Table 4.

Optical Surface	**Radius of curvature (mm)**	**Size/ Thickness (mm)**	**Material/ Coating**
Parabolic Mirror	101.6 CV	60 × 41/-	316-L stainless steel/Rhodium
Fold Mirror	flat	60 × 44/-	316-L stainless steel/Rhodium
Flat Steering Mirror	flat	170 × 80/-	316-L stainless steel/Rhodium
Window	flat	Ø = 48/8.0	Fused Silica
Window	flat	Ø = 48/8.0	Fused Silica

Table 4 Main specifications of KL14 endoscope's parts.

5.2 WAV Mirror Relay

The mirror relay (or referred to as transfer optics) enables all the camera systems included within the WAV line of sight to image the plasma and the plasma facing components from a position outside the TH. Since the WAV system includes cameras operating in the visible, near and middle infrared, this mirror relay covers from 300-3600 nm as a wavelength range (see [18]).

The optical path includes a near vertical light beam from mirrors M1 to M2, and then to M3 (see Figure 9). The goal behind it is to minimise optical aberrations by yielding near normal incidence on mirror M2, which is the only curved mirror in the relay. Minimising the aberrations is critical given the relative long physical distance between the plasma and the camera's optics. An intermediate image is formed after mirror M4 at a distance of 1.77 m farther along the light path with a diameter of 909.8389 mm as estimated by the optical model. This position is located in mid-air so there is no physical aperture during normal operations.

Outside the TH, there is a fused silica window (W1) and two folding mirrors, referred to as mirrors M5 and M6 which, in turn, relay the light to the multiple camera systems (see Figure 9). Initially, the design included three beam splitters (BS) after M6 in order to share the beam among the different camera systems operating in the visible, near infrared and middle infrared. However, by the final design these components were replaced by two dichroic-beam-splitters which minimises transmission losses and optimises the space available. The difference between a beam-splitter and a dichroic-beam-splitter is that a dichroic works by splitting the light as a function of wavelength independently of the intensity level whereas a beam-splitter divides the light beam by its intensity independently of the wavelength.

Table 5 shows some of the key parameters such as diameter, thickness and weight of the optical components that form the WAV relay up to the camera systems. The material

substrate for all the mirrors is fused silica (TSC3 Fused Quartz), the mirror grade is fine anneal, and they have an 'Enhanced Aluminium' coating. Regarding the radius of curvature (ROC), they are all flat with the exception of M2 which is a concave mirror with a ROC of -12000.0 mm. The two dichroic optics represented as D1 and D2 have a fused silica substrate and custom multilayer dielectric coatings on both sides. Finally, the window's substrate is infrared fused silica, optical grade A and fine anneal, and it is uncoated.

ID	Diameter (mm) + 0.00/ - 0.25 mm	Thickness (centre) (mm) ± 0.2 mm	Weight (kg) ± (0.01-0.1) kg
M1	150	25	0.97
M2	500	55	24.21
M3	300	38	5.88
M4	250	38	4.09
Window	280	20	2.70
M5	250	38	4.09
M6	300	38	5.88
D1	250	30	3.23
D2	250	30	3.23

Table 5 Some of the main parameters of the optical components of the mirror relay excluding the camera systems.

The function of the first dichroic (*i.e.* D1) is to reflect the visible wavelength range and transmit the near and mid infrared wavelength ranges. The function of the second dichroic is to reflect the near infrared wavelength range and transmit the middle infrared wavelength range. Specifically, dichroic optic D1 (see Figure 61) has on the front surface a high reflectivity (99%) coating for wavelengths between 0.4-0.7 µm as well as an anti-reflection coating for wavelengths between 0.9-1.2 µm and 3.0-3.6 µm on the front and back surfaces, all optimised for an angle of incidence of 15°. As for the second dichroic optic D2 (see Figure 61), the coating on the front surface is highly reflective for wavelengths between 0.9 and 1.2 µm and there is an anti-reflection coating for wavelengths between 3.0 and 3.6 µm on the front and back surfaces. The coatings have an expected 10-year operational shelf life.

The optical performance of the mirror relay was modelled using a paraxial lens to make an image for the camera system which is furthest away from the machine. Thus, isolating the mirror relay and excluding all the different final optics from the system. The beam diameter inside the relay varies from 96 mm at the fused silica window at the KL14 endoscope to 220 mm at the entrance of the penetration in the TH (see [18]). The main limiting factor for the performance of the mirror relay is the KL14 endoscope because the upper and lower fields form images that are not co-planar. The reason for being not co-planar is because the intermediate images produced by this type of design with tilted parabolic mirrors are not flat and also not co-planar. It should be noted that at the time the in-vessel mirror was designed, it was not envisaged the future design and installation of the mirror relay. On the other hand, the main advantage of the existing in-vessel mirror box was its simplicity in terms of the number of optical components required given its in-vessel location. Figure 13 presents the 'Through Focus Spot Diagram' for various fields (see [18]). The diffraction limit at a wavelength of 0.656 µm corresponds to an Airy diameter of approximately 10 µm. From Figure 13, it is possible to observe that on axis the image spots vary in size in between 10 and 45 µm. This translates into a pixel resolution of ~3 pixels, where the size of a pixel is assumed to be around 11.4 µm (see [19]). This pixel size was used as a baseline value since it was the pixel size corresponding to the on-vessel machine protection cameras at the time of the design. In terms of the spatial resolution, since 1 pixel corresponds to approximately 8 mm on the image, this means that spatial resolution is 24 mm.

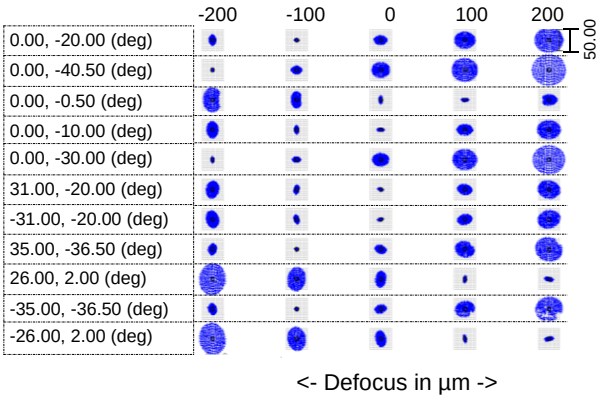

Figure 13 Through Focus Spot Diagram.

The Modulation Transfer Function (MTF) is presented in Figure 14, this shows the response of the mirror relay for the different fields as a function of the frequency response. The numbers at the top of Figure 14 represent the tangential and sagittal cases (TS) of the different field positions. The field positions are listed in the caption of this figure. The on-axis performance extends beyond 50 cycles mm^{-1} for 50% of the modulation which meets the requirements.

*Figure 14 Modulation transfer function for the WAV mirror relay. The numbers at the top represent the tangential and sagittal cases in degrees as listed here: **1**: 0.00, -20.00, **2**: 0.00, -40.50, **3**: 0.00, -0.50, **4**: 0.00, -10.00, **5**: 0.00, -30.00, **6**: 31.00, -20.00, **7**: -31.00, -20.00, **8**: 35.00, -36.50, **9**: 26.00, 2.00, **10**: -35.00, -36.50, **11**: -26.00, 2.00.*

The estimated Transmittance of the WAV relay based on the information sent by the suppliers is depicted in Figure 15.

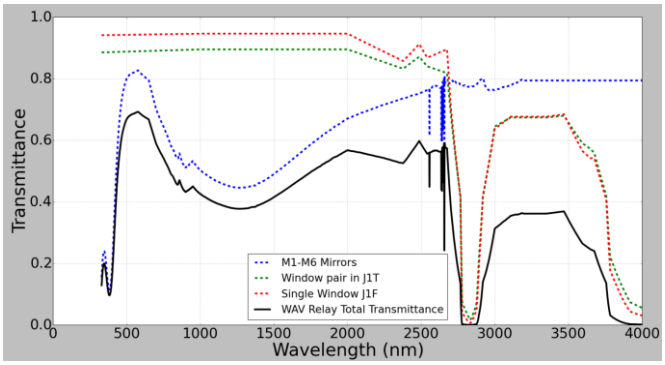

Figure 15 Estimated Transmittance of the Wide Angle View relay including the individual contributions from key components.

Figure 15 is comprised of several graphs. In black and continuous trace, the total transmittance of the relay as a function of the M1-M6 mirrors, the window pair in TH and the single window in J1F is plotted. This curve does not include the individual optics coupled to each individual camera system as this would only be representative for that particular camera diagnostic. The other traces presented with dashed lines corresponds to some other specific components listed on the legend such as the window pair in the TH (green dashed line) and the single window in J1F (red dashed line). The Enhanced Aluminium coating maintains a good reflectivity performance at longer wavelengths after the two narrow dips in transmission in between the wavelength range of 2.5-2.7 µm. The two narrow dips are considered an instrument artefact from the data provided by the supplier. On the other hand, there is a wide dip around 2.7-2.8 µm produced by the single window in J1F and the pair of endoscope windows on the machine, due to hydroxide absorption in the fused silica.

The major contribution to the total Transmittance comes from the combined throughput for the M1-M6 mirror set. The peak is reached at a wavelength around 576 nm for a value of 0.7. Transmittance drops to around 0.42 for the near infrared wavelength region around 1000 nm and it remains flat between wavelengths 3000-3500 nm but at a value of 0.36.

Furthermore, the estimated throughput including this time the dichroic performance supplied by the manufacturer is given in Figure 16. This throughput is shown for three wavelength ranges: visible, near and middle infrared. The throughput for the visible range is obtained as a result of the estimated transmittance of the relay together with the reflectance from the first dichroic (D1). Following from this, the estimated transmittance for the near infrared wavelength range takes into account the transmittance of the first dichroic, D1, and the reflectance of the second dichroic, D2. Finally, the response for the middle infrared wavelength range is obtained from calculating the transmission through the two dichroics (D1 and D2). The oscillations from around 1500 nm to 2500 nm wavelength range are due to the coating of the second dichroic.

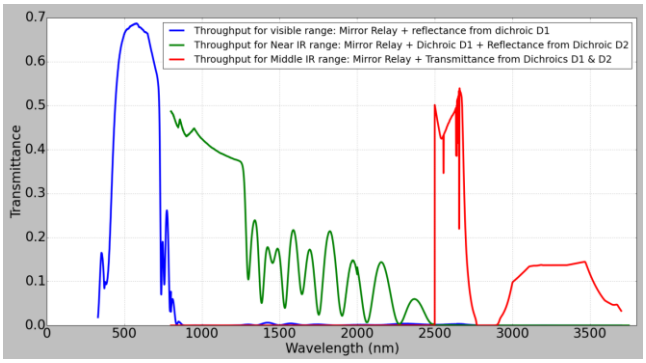

Figure 16 Estimated transmittance including dichroics performance for the visible (blue), near IR (green) and middle infrared (red) wavelength ranges.

5.3 Visible Cameras Cluster

The three visible cameras are KLDT-O5WB, KLDT-E5WD and KLDT-E5WE (see Table 1). They have been packed in a triangular cluster such that they are sharing the same line of sight (see Figure 17 and Figure 18).

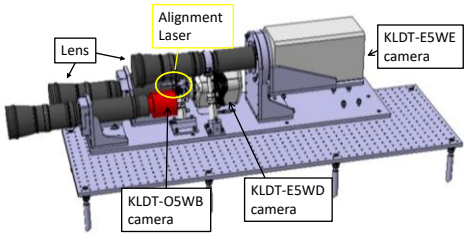

Figure 17 Underneath view of the visible cluster showing only KLDT-E5WD (spectroscopy camera) and KLDT-O5WB (operational).

Figure 17 and Figure 18 represent the computer-aided design (CAD) model showing the different mounting supports, base plates and the optical breadboards.

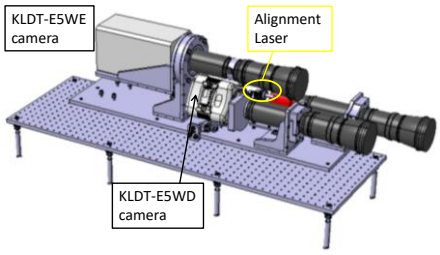

Figure 18 Above view of the visible cluster showing only KLDT-E5WE (high speed camera) and KLDT-E5WD (spectroscopy camera).

All these three visible cameras used the same model of camera lens. This is a telephoto lens with a focal length of 500 mm and the F# 5.6-11 when using the standard mount adaptor (model number is TP556ML and datasheet is provided in [20]). This lens is used in conjunction with aTX17-N Nikon F-C alternative mount adapter which extends the focal length to 850 mm with a maximum aperture of F# 9.6.

The resolution performance has been estimated for each of the three visible cameras (see Table 6) as the combination of the performance of the telephoto lens and the camera system and it is been displayed in terms of the number of pixels (see [21]). In addition, Table 6 also lists the 'Spatial Resolution' measured in millimetres per pixel for each of the three camera visible systems. A program called Calcam (see [22]) has been used to determine the spatial resolution by matching the field of view in CAD to images obtained. Since the visible cameras are imaging a WAV, the spatial resolution varies depending on the object depth of field: spatial resolution decreases with increasing object distance. It should also be pointed out that many tile surfaces are not normal to the viewing axis.

Camera System	**Resolution Performance (pixels)**	**Spatial Resolution (mm/pixel)**
KLDT-O5WB (operational)	1137 × 859	~ 3-9
KLDT-E5WD (spectroscopy)	414 × 313	~3 mm/pixel @ 1 m ~23mm/pixel @ 6.8 m
KLDT-E5WE (high speed)	390 × 295	~4 mm/pixel @ 1 m ~25 mm/pixel @ 6.8 m

Table 6 Resolution performance and spatial resolution for the visible cameras cluster.

5.4 Near Infrared Camera system: KLDT-P5WA

The camera lens for the KLDT-P5WA system was custom made by Sigma Koki Co. Ltd (https://www.global-optosigma.com/en_jp/). This is a mirror objective which consists of a Cassegrain optical geometry and a convex lens (see [23]) - three elements in total. The focal length is 830 mm with a 200 mm clear aperture. The design optimisation wavelengths are 600, 1000 and 1200 nm. Figure 19 shows a schematic of the KLDT-P5WA objective (see [23]) including the primary and secondary mirrors of the Cassegrain telescope and the lens. The filter, depicted after the lens, is positioned between the lens and the camera. This has the advantage of being able to use a more standard (smaller) filter size.

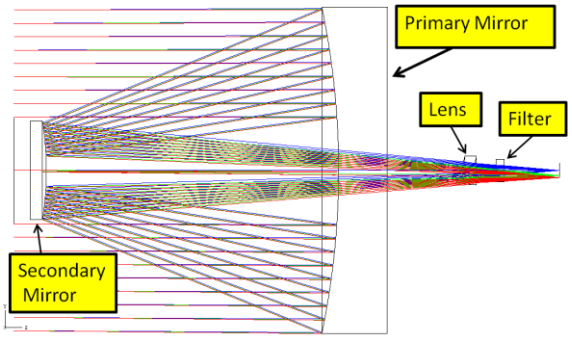

Figure 19 Schematic showing the ray tracing of KLDT-P5WA.

The 'Through Focus Spot' diagram for this system is shown in Figure 20. The performance is diffraction limited with a 6.9 µm Airy radius and at a distance of 19 m from the object. This design took as a camera system the current Hitachi camera sensor size at the time (see [19]).

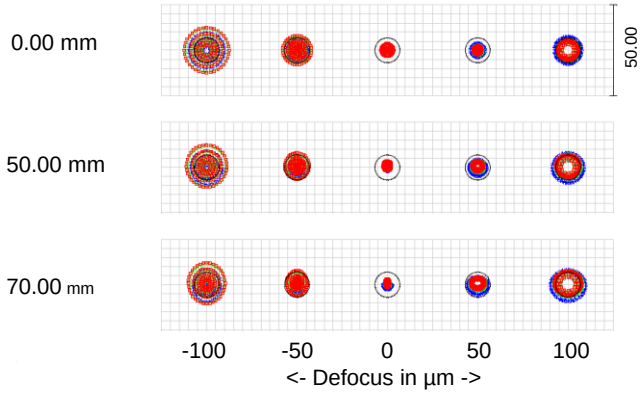

Figure 20 Through focus spot diagram of KLDT-P5WA objective.

The modulation transfer function is given in Figure 21. The maximum spatial frequency shown on the graph is 120 cycles/mm and it dips at 60 cycles due to the presence of the secondary mirror (see [23]). It also covers the wavelength range between 0.6-1.2 µm.

Table 7 shows the key parameters for the primary and secondary mirrors of the Cassegrain telescope. The material of the mirror substrate was specified as fused silica because of its low thermal expansion.

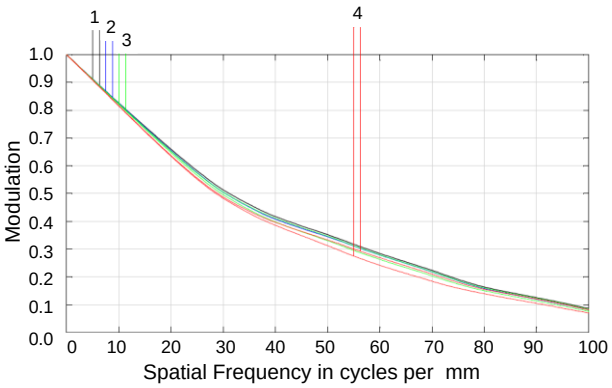

*Figure 21 Modulation transfer function for KLDT-P5WA lens. The numbers at the top represent the tangential and sagittal cases as listed here: **1** Diffraction Limit, **2** represents 0.00 mm, **3** represents 50.00 mm and **4** represents 70.00 mm.*

Regarding the manufacturing tolerances, the most critical one is the error in the ROC which cannot be higher than 0.1% (see [23]).

Mirror Element	Clear Diameter (mm)	Radius (mm)	Conic Constant
Primary	204	500.0 cc	-1.00
Secondary	62	192.1 cv	-3.04

Table 7 Cassegrain key parameters.

The material of the lens is N-BK7. Table 8 lists the key parameters. The design tolerances for tilt and decentre are ±0.20° and ±0.20 mm respectively. The tolerancing provides an 80% probability that the Root Mean Square spot radius is around 13 µm.

Lens Element	Radius (R) (mm)	Centre Thickness (mm)	Clear Aperture (mm)
Lens	26.58 cx	7.0 ± 0.1	18
	21.13 cc		16

Table 8 Lens key parameters.

5.5 Middle Infrared Camera system: KLDT-E5WC

The camera lens for the KLDT-E5WC system was custom made by Sigma Koki Co. Ltd (https://www.global-optosigma.com/en_jp/). This is an F/3 objective with a focal length of 600 mm (see [24]). It consists of a Cassegrain telescope with four lenses. The position for the optical filter is in between the third and fourth lenses (see Figure 22). In addition, the optical model includes a 'cold stop'. The 'cold stop' is an aperture located in front of the camera sensor and its purpose is to prevent any spurious thermal contribution from reaching the sensor.

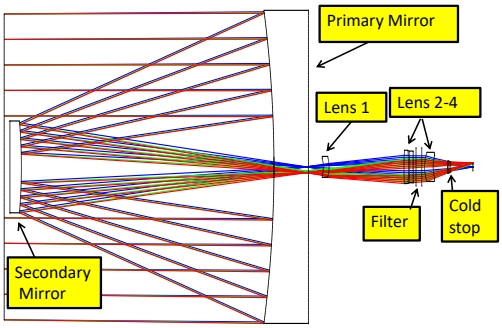

Figure 22 Zemax layout of the of the mid wavelength infrared for KLDT-E5WC.

This design has been optimised for a cold stop of a diameter of 6.56 mm and located at 19.4 mm from the detector. The focus can be adjusted by ±2 mm if the distance between the fourth lens and the cold stop is changed by ±1 mm. The performance is diffraction limited with an Airy disc radius of 12.97 µm at a wavelength of 3.6 µm (see Figure 23).

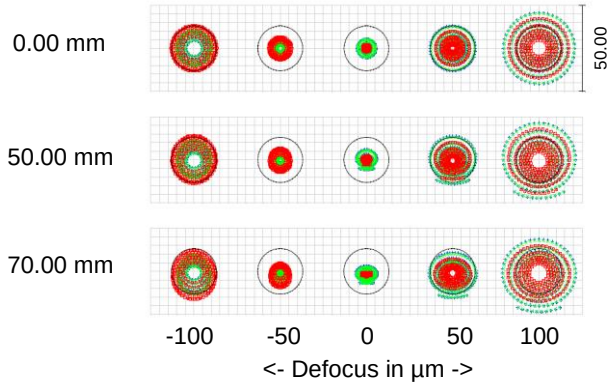

Figure 23 Through focus spot diagram of KLDT-E5WC.

The MTF curve presents a maximum spatial frequency is 100 cycles mm^{-1}. The slope in the MTF curve reduces around 30 cycles mm^{-1} and this is produced by the secondary mirror (see Figure 24).

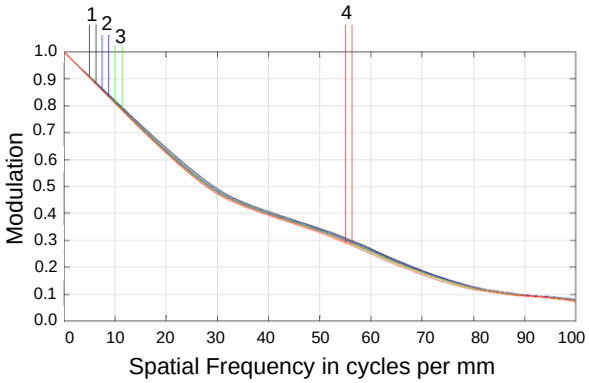

*Figure 24 Modulation transfer function of KLDT-E5WC. The numbers at the top represent the tangential and sagittal cases as listed here: **1** Diffraction Limit, **2** represents 0.00 mm, **3** represents 50.00 mm and **4** represents 70.00 mm.*

The key parameters of the primary and secondary mirror of the Cassegrain are listed in Table 9. For the primary and secondary mirrors of the Cassegrain, the most critical parameters are the tolerance on the ROC (ΔR) and the irregularity measured in fringes. Any deviation in the ROC had to be lower than 1% for the primary mirror and lower than 3% for the secondary mirror. As for the irregularity of the mirror surface, it cannot be higher than ±1 fringe. Noted that the test wavelength of the tolerance values in Zemax is 0.6328 µm.

Mirror Element	Clear Diameter (mm)	Radius (mm)	Conic Constant
Primary	205	600.0 cc	-1.000
Secondary	61	262.0 cv	-4.593

Table 9 Key parameters of the Cassegrain mirrors.

The key parameters for each of the refractive elements is reported in Table 10. The material for the lenses is Silicon with the exception of the third lens which is made of Germanium. These two materials were selected to optimise the transmission in the mid-infrared region. The combination of the two material yields an athermal design for the target wavelength range. Regarding the design tolerances, the most significant parameter is the deviation from the ROC of the second lens element which was specified as ≤ 1%. In addition, the tilt and decentre and axial position tolerances are ±0.10° and ±0.10 mm for all the lens elements respectively. These values ensure an 80% probability that the performance is diffraction limited with an Airy disc radius of 13 µm.

Lens Element	Radius (mm)	Centre Thickness (mm)	Clear Aperture (mm)
Lens 1	16.63 cc	5.0 ± 0.05	11
	19.25 cv		14
Lens 2	117.7 cv	4.0 ± 0.1	22
	117.7 cv		22
Lens 3	97.27 cc	3.0 ± 0.1	21
	flat		21
Lens 4	24.09 cv	7.5 ± 0.1	19
	24.09 cv		15

Table 10 Key parameters of KLDT-E5WC lenses elements (cc: concave, cv: convex)

6. Mechanical Design of the Mirror Relay inside the Torus Hall

The relay optics in the TH which transfers the light to outside the biological shield wall had to be supported by custom designed engineering structures as shown in Figure 25 below. The key requirement for these structures was to ensure they were sufficiently rigid and stable to maintain the optical alignment in the presence of magnetic fields during the experimental campaign.

These structures are fixed to the vertical limb of the transformer. The designs were subject to a structural analysis in order to assess the stress levels from self-weight and operational magnetic forces to evaluate if they will be fit for purpose. It was also important to consider the level of electrical conductivity for the selection of materials. Furthermore, for the largest mirror (*i.e.* M2), it was not possible to use a standard off the shelf mirror mount, which are only scarcely available at the size required but critically only available made from aluminium or stainless steel, due to the engineering analysis simulations predicting significant eddy currents induced by the JET magnetic fields. These eddy currents can, in turn, induce forces that potentially can shift or even worse distort and break the mirror mount as well as the supporting structures; therefore, affecting the performance of the mirror relays. As a result, the main material used is Glass Reinforced Plastic (GRP) to entirely avoid eddy currents for this mirror. A bespoke gimbal mount for the large M2 mirror made of GRP was designed in house and manufactured externally.

The mirrors inside the TH are grouped into two mechanical mirror support assemblies which are known as 'M1&M3' and 'M2&M4' assemblies. As the name implies, M1&M3 contains mirrors M1 and M3 and it is the same principle for the M2&M4 mirror assembly. This section presents the engineering analysis of each of these mounting frames as well as the mirror mounts. In addition, due to the mechanical decoupling of the optics from the endoscope, modelling of the vacuum vessel and endoscope's movement was also performed. The calculations yielded a 1 mm upwards movement from the vessel due to divertor coils forces during a pulse. This translates in a 0.25 mm upwards shift of the endoscope and 0.1 mm radially outwards movement (see [25]). The radial movement was not considered an issue for the optical performance. As for the upwards shift, the optical design provides sufficient flexibility for compensating for this level of upwards shift.

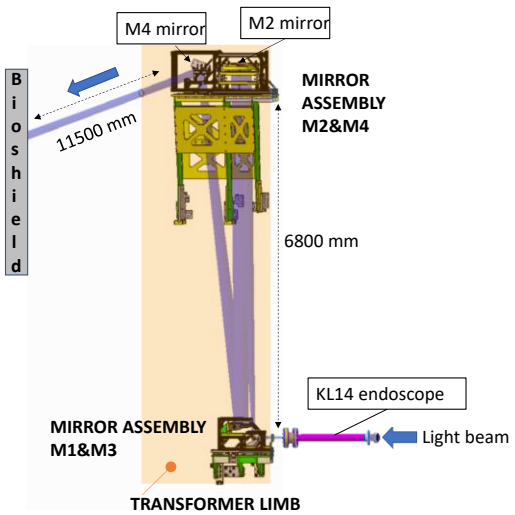

Figure 25 Diagram of the WAV M1&M3 and M2&M4 assemblies.

Figure 26 shows a photograph taken of octant 5 with the WAV installations labelled; this was taken at a time when the M1&M3 mounting frame had the protective plastic cover on just after just installation.

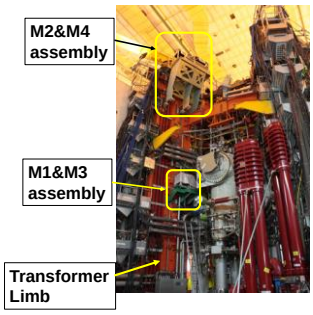

Figure 26 Photo of the WAV M1&M3 and M2&M4 support platform and mounting frame assemblies during the in-vessel intervention (i.e. many JET components removed).

6.1 WAV-M1&M3 Mirror Assembly

Starting with the M1&M3 assembly (see Figure 27), its dimensions are width of 543 mm and length of 1600 mm. The total weight is 400 kg. It is mounted as shown on Figure 25 and Figure 26 underneath the mirror assembly M2&M4 on the vertical side of the transformer limb 4-5. It consists of three main parts (see Figure 27): the 'Optical Cage' assembly made from aluminium extrusion, the 'Mounting Platform' assembly made of GRP and the steel brackets fitted to the limb (denoted as 'limb brackets').

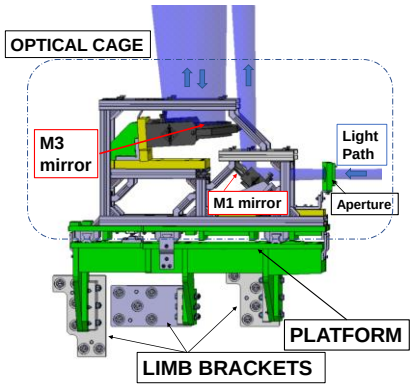

Figure 27 Diagram of WAV-M1&M3 assembly showing the light path.

6.1.1 WAV-M1&M3 – Optical Cage assembly

The 'Optical Cage' refers to the outside frame around the mirrors and their supports and provides rigidity for the optical sub-assemblies. The weight of the complete mounting frame is 161 kg. The diameters of the mirrors M1 and M3 are 150 mm and 300 mm respectively. The mirrors are mounted on aluminium gimbal mounts supplied by Aerotech (https:\\www.aerotech.com). The specific models for the M1 and M3 mirror mounts are AOM110-6 and AOM110-12 respectively (see [26]). There is an aperture on the front of M1&M3 which has a circular shape with a diameter of Ø = 50 mm and is positioned before M1 in the light path. The aperture consists of a GRP ring made of trade name Durostone® EPC203 (see [27]) and a metal base made of aluminium alloy. The base is then fixed to a Durostone® EPM203 (see [28]) plate to avoid eddy current loops. The M1 gimbal mirror mount is mounted onto a bent plate with an angle of ~ 47° to be set the nominal angle for the trajectory of the light path. The bent plate's material is stainless steel because of its low magnetic permeability, higher stiffness and lower conductivity compared to aluminium alloy. The stainless steel plate is in turn, fixed to a GRP base. A photo of the M1&M3 'Optical Cage' assembly before being transported to the TH is presented in Figure 28.

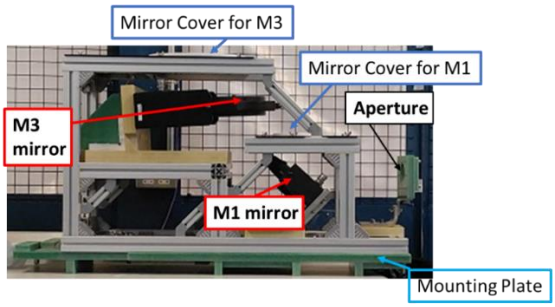

Figure 28 Photo of the Optical Cage for WAV-M1&M3 after being assembled in the lab prior to installation in Torus Hall.

Secondly, mirror M3 is installed with the surface plane horizontally to reflect the light path originating from M2 above back up towards mirror M4. The key dimensions of the WAV-M3 sub-assembly are 685.5 mm × 276.2 mm × 523.4 mm. As depicted in Figure 29, the gimbal mount is fixed to the support which is made of GRP in order to avoid eddy current loops. The mounting sub-assembly is shown with parts in three different colours to represent different types of materials in use. The L-shape support coloured in light brown is made of EPM203 (see [28]). The two ribs in green colour are made also of GRP with trade name Durostone® EPC203 (see [27]). Helicoil inserts are used in the tapped GRP fixing holes to avoid risk of thread-stripping.

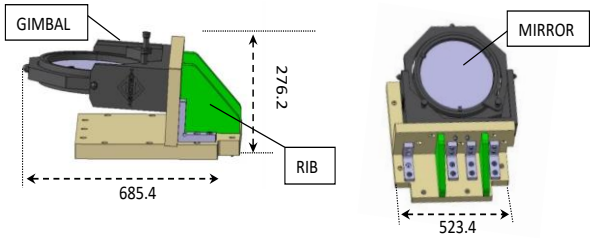

Figure 29 Diagram showing two views of the M3 sub-assembly with key dimensions in millimetres.

The surrounding 'Optical Cage' is shown in Figure 30. Three different views are presented, first without the dust and mirror covers, secondly with only the dust covers and thirdly with the dust and mirror covers which were used during transportation and installation into position. The 'Optical

Cage' is a modular structure which consists of different extrusion profiles made of aluminium alloy 6082 T6. The plates coloured in light brown represent the GRP components. The frame consists of 334 parts excluding the GRP plates. The weight of the frame is 38.9 kg excluding also the GRP plates. The dust covers were left permanently once the assembly was installed. Both covers are made of polyethylene. They were custom made and supplied by Roechling (https://www.roechling.com/).

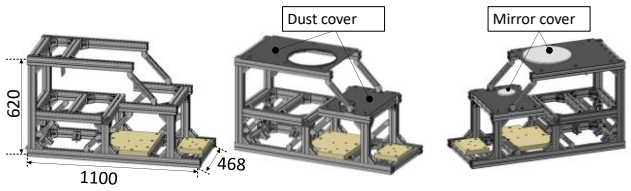

Figure 30 External frame of WAV-M1&M3 Optical Cage showing dust and mirror covers as well as key dimensions in millimetres.

Thin plates made of Durostone® EPM203 were inserted in between joints of the 'Optical Cage' and fixings at these joints were fitted with insulating bushes to avoid eddy current loops during a pulse. The thickness of these isolating plates is 3 mm. The insulation bushes were made of Durostone® EPR S1 (see [29]).

The 'Optical Cage' is fitted on three carriages which run on three rails installed on the 'Mounting Platform' assembly. This provides the mirror frame with the capability of docking and undocking from close to the limb. This additional function was introduced in order to provide sufficient clearance for the installation of the 'Boom Tent' during maintenance periods, (*i.e.* when the machine is not operational). The 'Boom Tent' houses a remotely operated robot which carries out repairs and/or upgrades inside the vacuum vessel (see [30]). At the end of the maintenance periods, the 'Boom Tent' is removed from the TH and the M1&M3 mirror frame is moved back to its nominal position within the optical relay. The manufacturer for the linear sliding carriages and rails was Parker Origa (http://www.parkeroriga.com). The sliding range can reach a maximum of 130 mm. The design incorporates three locating positions, which can be set up by the 'Location Pin' which is spring loaded and made of A2-70 stainless steel.

In addition, there are three locking tabs to brace this sliding assembly from undesirable movements in the plane of the mounting platform surface when it is in the operations position and two sliding stops to ensure the 'Optical Cage' does not move outside its sliding range (see Figure 31) when docking/undocking.

6.1.2 WAV-M1&M3 Mounting Platform assembly

The 'Platform Assembly' (see Figure 31) is all made of GRP whose trade name is Durostone® EPC203 (see [27]). The weight of the complete 'Platform Assembly' is 128.8 kg. It consists of the baseplate where the sliding mechanism is mounted onto, three mounting legs with three limb stiffening legs (see Figure 32). These stiffening legs are sandwiched in between the mounting leg of the 'Platform Assembly' and the limb brackets. In addition, there are a number of ribs and base plate stiffeners to provide sufficient strength to the whole structure.

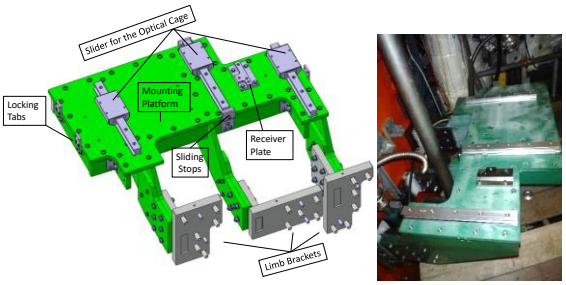

Figure 31 Left: Platform Assembly and the limb brackets. Right: Photo taken during installation.

An engineering analysis of the stresses under load from the optical cage combined with self-weight was carried out on the 'Platform Assembly' and limb brackets (see [31]).

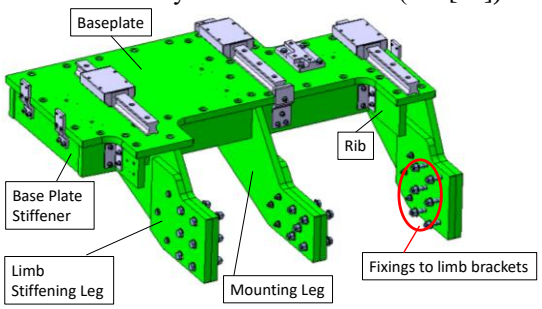

Figure 32 Main GRP components of the M1&M3 Platform Assembly

For this analysis, the 'Optical Cage' was modelled as a point mass placed on top of the platform surface. The limb T-bracket flanges (see Figure 34) are not included in the model, but the T-bracket webs (see Figure 34) are connected to the platform and fixed on the faces that are welded to the T-bracket flanges. The force and moment reactions resulting from the finite element analysis were then used in a separate weld analysis for the T-brackets. Figure 33 illustrates that the maximum stress level is 9 MPa for the GRP platform and the maximum deformation is 0.2 mm.

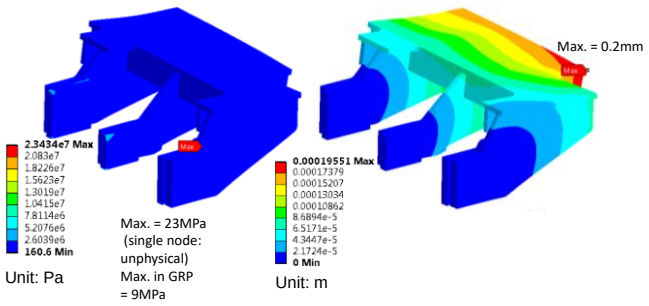

Figure 33 Stress levels and deformation for WAV M1M3 (see [31]).

6.1.3 WAV-M1&M3 Limb Brackets assembly

The three limb brackets (see Figure 34) are fixed to the vertical side of the limb. These limb brackets are known as 'Left Hand Side' (LH), 'Right Hand Side' (RH) and 'Middle'. Each of them has got a different shape in order to adapt to the available space left by the existing equipment on the limb. The weight of the three limb brackets all together is 109.41 kg. The limb brackets are made of Stainless Steel 316L. Each limb bracket consists of two plates: the flange plate bolted onto the limb and the web plate which is attached to the platform assembly. The T-bracket webs are welded to the flanges attached to the limb.

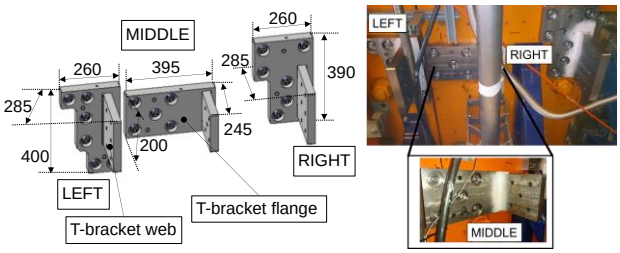

Figure 34 Left: Models of the three limb brackets with key dimensions in millimetres. Right: Photos taken after the limb brackets were installed.

The engineering analysis was carried out for each limb bracket applying the respective individual force and moment reactions from the modelling of the mounting frame. In addition, a global sanity check was performed using the overall loads. The boundary condition in the analysis does not include the constraint of the entire surface in contact with the transformer limb. The calculated Von Mises stresses and total deformations for each of the flanges are considered acceptable (see [31]).

6.2 WAV-M2&M4 Mirror Assembly

The WAV-M2&M4 assembly is also installed on the vertical side of the limb in the Torus Hall, on top of the WAV-M1&M3 assembly. The M2&M4 mirror assembly has the following dimensions: 980 mm × 2125 mm × 2380 mm. It consists of three components: the tower, the brackets that attach the tower to the limb, denoted as 'limb brackets', and the optical mirrors and the envelope frame around the optical components also referred to as 'Optical Cage' (see Figure 35). The tower is made of GRP and weighs 602 kg. The tower acts as the base platform for the optical cage. This section will start by describing the top sub-assembly (*i.e.* 'Optical Cage'), followed by the 'Tower' and 'Limb Brackets' sub-assemblies.

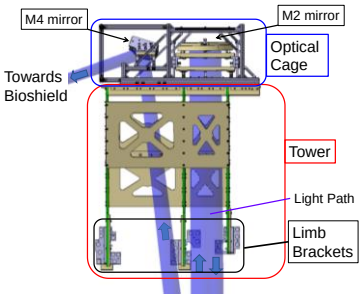

Figure 35 WAV-M2&M4 sub-assemblies.

6.2.1 WAV-M2&M4 – Optical Cage assembly

The optical cage refers to the frame which contains the two mirror sub-assemblies: M2 and M4. The overall dimensions are 2136 mm × 1003 mm × 820 mm. The M2 assembly which includes the mirror itself, and the mounting support is on the right-hand side of the optical cage and the M4 assembly is located on the left-hand side as viewed from octant 5 of the machine.

The M2 mirror is the only mirror in the WAV relay which is not flat, it is also the largest in diameter and the one which is mounted on a novel kinematic mount made of GRP. It was not possible to use a commercial mirror mount because the analysis of static stresses and ERFA kicks (see [32] and [33]) demonstrated that the material of the mirror mount could not be metallic. The predicted level of eddy loads acting on a standard metallic mirror mount of such a large diameter would potentially deform the mount and therefore misalign the mirror as well as in the worst-case scenario causing irreversible damage to both (*i.e.* the mirror and the mount). Consequently, it could only work with an insulating material. Note that ERFA kicks (see [33]), used in some JET experiments, are periodic voltage pulses applied to the radial magnetic field circuit causing magnetic field changes that perturb the plasma vertical position Their periodic nature has the potential to cause vibration and excite resonances in mechanical assemblies. The only metallic components are the fixings, all the GRP material is Durostone® EPM203. As far as the authors are aware, this has not been done before on a fusion machine. The assembly of the parts was carried out in-house. Concerns that the hygroscopic nature of GRP might lead to dimensional and thus optical alignment changes in-service have proved unfounded, even during non-operational periods where temperature and humidity are not well controlled. The overall dimensions of the M2 assembly are listed in Figure 36 as well as showing the two main sub-assemblies. The optical mirror is facing downwards towards M1&M3 assembly. Thus, Figure 36 depicts the back (non-optical) surface of the M2 optic. All the components coloured in light brown represent the GRP material which in this case is Durostone® EPM203 (see [28]).

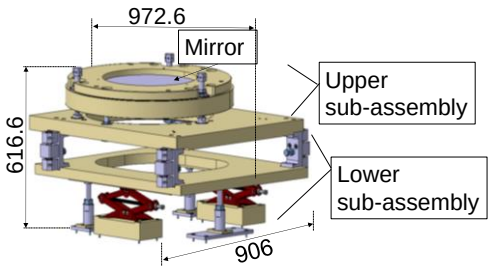

Figure 36 M2 mirror assembly showing overall dimensions in millimetres and the main sub-assemblies.

The 'Upper sub-assembly' consists of 'Floating Ring' and 'Mounting Plate' sub-assemblies. The overall dimensions are reported on Figure 35. The mass of the 'Floating Ring' is 33 kg and the 'Mounting Plate' is 54 kg.

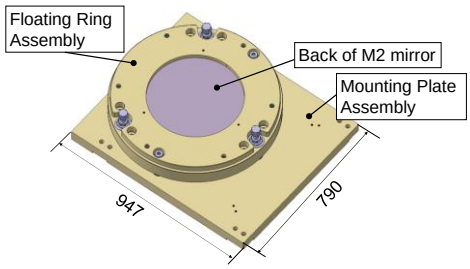

Figure 37 Floating Ring and 'Upper Mounting Plate sub-assembly' of the M2 structure. Overall dimensions are in millimetres.

The M2 optic is captured by the Floating Ring (see Figure 37). It consists of two rings sitting on top of each other and the actual mirror is in between. In addition, the mirror is resting on three equidistant contact points on the bottom ring (see Figure 38). They are 2mm deep semi-circular recesses on the inner side of the ring and a pad of the same shape with a diameter of 35 mm and 3 mm thickness was inserted onto each of them by pushed fitting. They are also made of Durostone® EPM203. In addition, three nylon-tipped grub screws secure the mirror in line with the pads on the top ring (see Figure 38 and Figure 39). Figure 38 presents the top and bottom rings including front and back views of the top ring. The thickness of the rings is 35 mm. In order to prevent the mirror moving sideways inside the assembly, there is also one grub screw on the inner side of the bottom ring. The grub screw is inserted by a M8 size Helicoil.

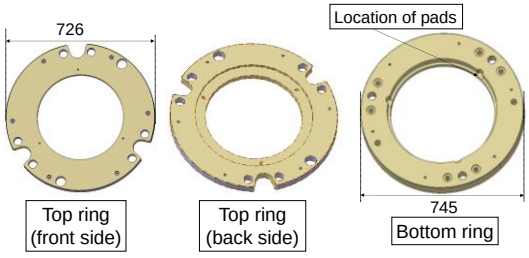

Figure 38 Top and bottom rings from the Floating Ring sub-assembly of M2. (Dimensions in millimetres).

The fixings and the alignment screws attach the 'Floating Ring' sub-assembly to the 'Mounting Base Plate' sub-assembly. The alignment screws are the ones which enable the optical alignment of the mirror M2. The alignment screws together with the 'Upper Assembly' constitutes the novel kinematic mount made in GRP. In general, a kinematic mount has three points of contact using a cone, a v-groove and a plane surface mating contact respectively (see [34]) positioned so as to form a triangular shape. This enables the tilt of the mirror around its centre axis. The kinematic mount avoids over-constraint of the system, with each degree of freedom constrained only once, but has the disadvantage that angular adjustment of the mirror is accompanied by some translation.

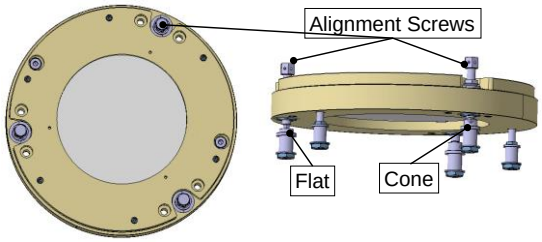

Figure 39 Top and side view of alignment screws on 'Floating Ring Assembly'.

Each of the three alignment screws is formed of two parts: hexagonal screw and the 'alignment ball'. Figure 40 presents a cross section of the key components and how they connect the 'Floating Ring' assembly with the 'Mounting Plate' assembly. The dimensions of the complete adjustment screws are 36 mm × 184 mm. The screws themselves (*i.e.* without the balls) are made of A2-70 stainless steel. The end of each screw part has a hole to be able to insert the 'Alignment Balls' with a press fit (*i.e.* the mating part). The dimensions and shape are given in Figure 40. The 'Alignment Balls' (see Figure 40) are made of UHB Arne steel (hardness class: 59 HRC) and weigh 40 g each. This material is an alloy steel typically used for the making of tools which is known for its hardness and high yield stress, making it capable of withstanding Hertzian near-point-contact stresses without plastic deformation, and resistance to chipping (see https://en.wikipedia.org/wiki/Tool_steel#Oil-hardening:_the_O_series). Galvanic corrosion due to the interface of dissimilar metals is not anticipated due to the controlled atmosphere of the TH.

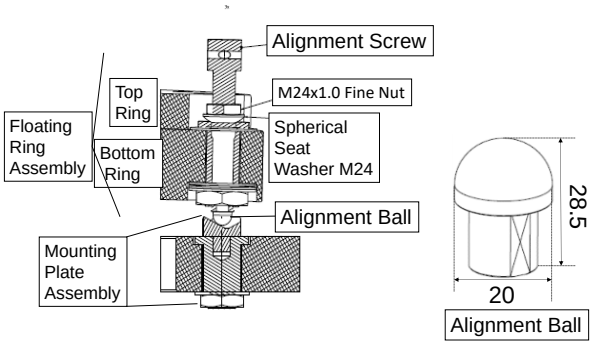

Figure 40 Left: Cross section of Alignment screw fitted through the 'Floating Ring' Assembly and the 'Mounting Plate' Assembly. Right: Alignment Ball. Dimensions in millimetres.

The 'Alignment Screws' are then fitted into the 'Floating Ring Assembly' using a threaded bush with a M24 × 1.0 mm nut. The threaded bush is made of stainless steel A4-80 1.4401 (316) and the nut is made of A2-70 stainless steel. As a kinematic mount, there are also here the cone, v-groove and the plane surfaces, each acting as the mating contacts for each of the alignment screws where the 'Alignment Ball' rests. The dimensions and shape of each of these contact points are provided in Figure 41. The spherical seat washers accompanying the alignment screws prevent the screws from 'binding up' as they are adjusted. Additional hole positions were added to the design for the retro fitting of springs in order to provide additional constraint. However, this was not needed when the mirror relay was in operation –gravity provides sufficient downward force to securely locate and hold the 'Floating Ring Assembly'.

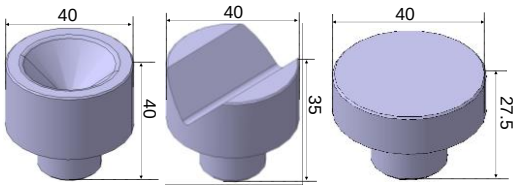

Figure 41 Dimensions (millimetres) and shape of the three kinematic contacts: cone, vee and flat respectively.

There is a pair of fasteners located opposite each other which have the function of locking the connection of the Floating Ring to the Mounting Plate after adjustments have been completed (and to secure for lifting operations). The material is also stainless steel A4-80 1.4401 (316). In addition, there are six fixing bolts - a standard M10x40 Hex Socket Head Cap which are used to fix the two rings from the 'Floating Ring Assembly' together. Just below the 'Floating Ring Assembly' and within the 'Upper Sub-Assembly', there is the 'Mounting Base Plate' (see Figure 42). The dimensions of this plate are 947 mm × 790 mm × 55 mm. The material of the plate is the same as the floating rings (*i.e.* EPM203).

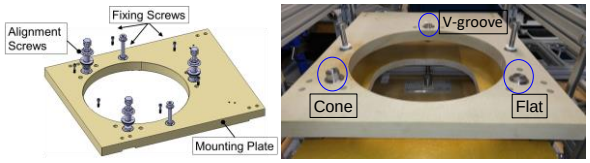

Figure 42 Left: Alignment screws and fixing bolts on the 'Mounting Base Plate'. Right: Photo of the 'Mounting Base Plate' showing also the three kinematic points.

The 'Lower sub-assembly' as depicted in Figure 36 and Figure 43 provides the capability of making relatively coarse adjustments of the height of the M2 mirror for focussing the relay. The main parts are 'Y Base Plate', scissor jacks (×2), jacking pads (×2), jack screws (×3), insulating plates (×3) and a 'linear bearing unit'. The opening in the middle of the 'Y Base Plate' is for the light path on M2 mirror. The adjustment of the height is provided by two scissor jacks at both sides of the 'Y-BasePlate'. The locking screws on the mirror clamp blocks are then engaged and the jack screws are set to provide failsafe support of the assembly, allowing the scissor jacks to be removed. The plate material is the same as the rest of the assembly: EPM203.

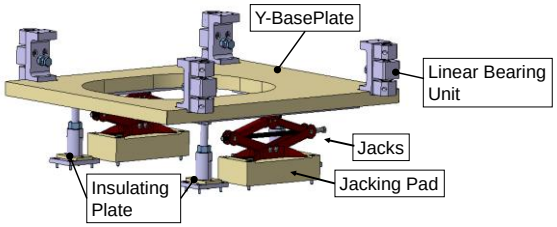

Figure 43 Key components of the 'Lower sub-assembly'.

The overall dimensions are listed in Figure 44. The scissor jacks need to be operated manually. However, it was not found to be necessary to use them during the alignment phase since the initial height was acceptable. The forces provided by the jack screws are distributed evenly using metal plates which are described as 'Load Spreader Plates' (see Figure 44). There are three of them and they are all made of stainless steel 1.4404 (316L). These plates are attached to the 'Y-BasePlate' by using M8 size fixings with Helicoils. On each of the four corners of the 'Y-BasePlate', there is a bracket unit which consists of two linear bearing units to guide the vertical movement and a mirror clamp stop which are fixed to a C-shape bracket denoted as 'Linear Bearing Housing Leg' (see Figure 44). The linear bearing unit's part number is 'LUHR 25' which can be found from RS (https://uk.rs-online.com/web/p/linear-ball-bearings-bearing-units/2849380/). In between the two linear bearing units, there is the 'Mirror Clamp Block' that is locked to secure the aligned height of the sub-assembly. The material is stainless steel 316L and it is attached to the 'Y-BasePlate' at the bottom and the 'Mounting Base Plate' on top using two bolts size M8 each side. The jack screws were designed to support evenly

each side of the 'Y-BasePlate'. The specified material for all these fasteners is A2-70 stainless steel. The bolt head rests on the 'Load Spreader Plates' located in the underside of the Y-Base Plate and forming a triangular shape (see Figure 44 and Figure 43). The base sits on top of an insulating plate which is also made of EPM203 which, in turn is attached to a slightly larger metal plate made of stainless steel. The insulating plate is fixed to the 'Load Spreader' (see Figure 44). The 'Load Spreader' plates are then mounted onto the 'Mounting Base Plate' of the M2 Tower which is described in more detail in the next sub-section.

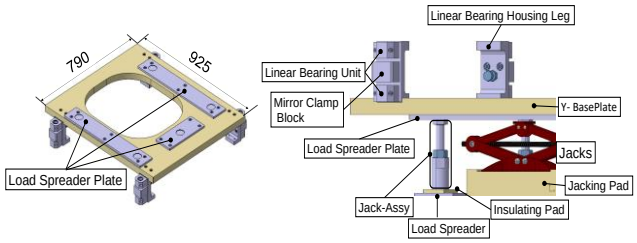

Figure 44 Left: Underside of Y-Base Plate. Dimensions in millimetres. Right: Detailed list of components within the 'Lower sub-assembly'.

An engineering analysis of the stresses and respective deformation for the M2 optics within the WAV-M2&M4 assembly is reported in [35]. Since the mirror is sitting flat and horizontal over the kinematic mount, gravity helps to keep the mirror in this position. The direction of deformation to analyse is the vertical deformation. The results yielding the vertical deformation levels of the M2 kinematic mount plus the M2 mirror itself are given in Figure 45.

The largest value is 0.039 mm and in the vertical direction. This is considered a small value and may be partly due to contact 'settling' in the model. The different colours give an indication of the deformation levels. The location corresponding to the peak deformation is labelled with a red arrow and it is in between the floating ring and the base plate. An analytical calculation to determine the level of distortion within the GRP ring itself was also carried out as well. The assumptions included in the calculations consider the GRP material as isotropic using the worst case of orthotropic elastic properties (see reference [35]). The values obtained from the analytical calculation are regarded as acceptable. In addition, the maximum stress levels corresponding to this level of deformation was 0.094 MPa which is not considered significant.

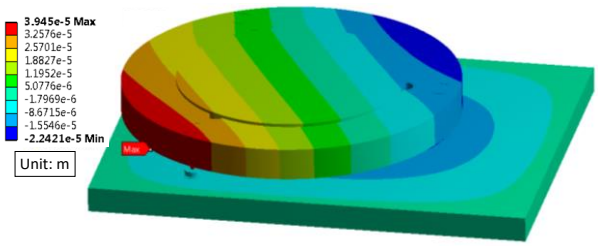

Figure 45 Vertical deformation of the M2 kinematic mount with mirror. The deformation peak is shown with a red arrow.

The kinematic contact points (*i.e*. cone, vee and flat) were also analysed (see Figure 46 and reference [35]). The status of these three kinematic contact points was classified as: 'Over Constrained', 'Far', 'Near', 'Sliding', 'Sticking' and each of this status was given a different colour. The results are also considered acceptable since the contact patterns are as expected (*i.e.* free to respond to adjustments) and none of the kinematic points appeared to be over constrained or sticking which are the two far extreme situations (see Figure 46).

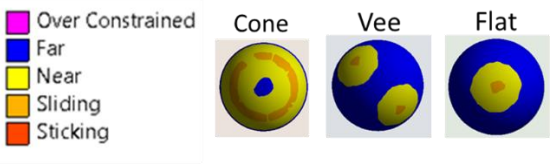

Figure 46 Contact status of the kinematic contact points.

The second mirror assembly within the optical cage of WAV-M2M4 is the M4 sub-assembly (see Figure 35). This includes the optical component and the supporting mounts. The mirror M4 is located next to M2, and it is responsible for directing the light path towards the WAV penetration in the biological shield wall.

The main components of the mounting support for mirror M4 are given in Figure 47. M4 is mounted on a bent plate bracket with an inside angle of 120°. The inside bend is supported by three ribs, and it is all fixed onto a short pedestal. The material for all the metallic components apart from the M4 gimbal mount is stainless steel (316L). The 'Baseplate' which is in between the 'Angled Bracket' and the supporting legs is made of Durostone® EPM203 (see [28]). In addition, there are also insulating plates made of the same material as the baseplate which are not visible in either of the two figures below but have been inserted underneath the supporting legs. The M4 gimbal is attached to the back of the angled bracket (see Figure 47). This gimbal is made of anodised aluminium (Model: AOM110-10) from Aerotech (https:\\www.aerotech.com). The datasheet for this gimbal mount can be found in [26]. The supporting legs have each been braced by fixing two supporting brackets. The fixings size is M8 except for the ones used in the supporting legs which are M10.

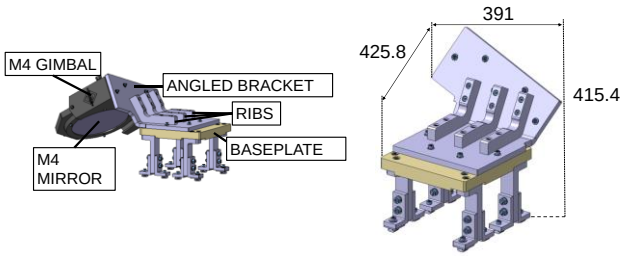

Figure 47 Left: M4 key parts. Right: M4 mounting bracket with dimensions in millimetres.

The engineering analysis for the M4 mirror assembly has focus on the frequency response due to the metallic gimbal mount (see [35]). In the model used, the mirror M4 is represented as a point mass in the centre of the gimbal. The model also assumes a damping level of 5%. Figure 48 shows the levels of distortion as a function of colour with the two extremes depicted in red and dark blue. Translating these values into pixels, it gives the result of ±1.8 pixels which corresponds to a tilt of ±0.023° which is slightly lower than the maximum tolerance specified for the optical design for M4 which is ±0.05°.

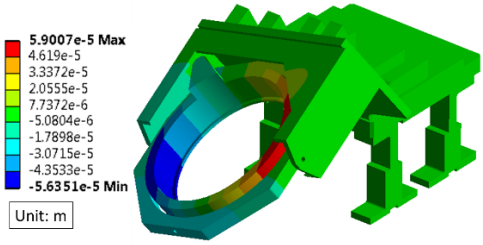

Figure 48 Deformation levels for the worst case mode showing the values represented by different colours of M4 mirror assembly.

The frame surrounding the M2 and M4 mirror (see Figure 49) assemblies is made of modular aluminium extrusion beams. It does not serve any structural function but just delimits the space envelope around the M2 and M4 mirror assemblies and supports protective covers. The dimensions are: 2136 mm × 942 mm × 808 mm and it weighs 89.9 kg. The material of these strut profiles is aluminium alloy. The 'Optical Cage' was built with different strut profile parts accounting for a total of 31 of them. Each of these profile parts is connected together with a corner bracket and there are 45 of them in total. The fixings size is M8. In order to avoid the formation of eddy current loops, there are a series of insulating plates of different sizes made of GRP at different joints. Since this frame does not hold any significant weight or support any significant loads, it was not necessary to perform an engineering analysis.

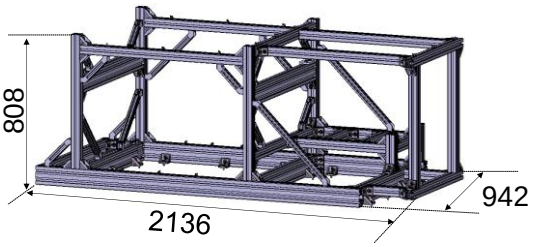

Figure 49 Front View of optical cage frame with dimensions.

As mentioned earlier, a series of protective covers were designed to be positioned on top and below the mirror assemblies (not shown in Figure 49). The material is polyethylene. In addition, two more covers were designed for the underside of the optical cage to protect the optics during transportation lifting operations and installation.

6.2.2. WAV – M2&M4 Tower or 'Mounting Platform'

The 'Tower' as it is commonly referred to, represents the supporting platform for the 'Optical Cage'. Figure 50 gives a front and a back view of the tower with main dimensions. The most striking feature of this structure is its height, slightly less than 2.5 m.

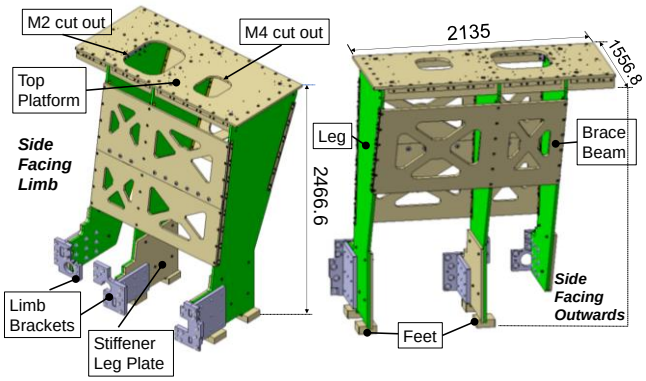

Figure 50 Side facing the limb and the side facing outwards of the WAV-M2&M4 GRP tower with overall dimensions in millimetres.

Due to the relative long distance between the pair of mirrors M1&M3 and M2&M4, the first thought was to mount from the upper section of the limb. However, it was estimated that the outboard upper section of the limb can move by approximately 5 mm during a pulse (see [36]). This instability is due to the thermal expansion of the central stacks of the poloidal field coil P1 during a JET pulse. The temperature increase could rise to 40 °C. Consequently, only the vertical section of the limb could be used for mounting components onto it. Since the position of the optics could not be moved because that will affect the optical performance of the relay, the only option was to construct a tower that will be fixed at the section of the limb which was stable enough to locate the optics according to the requirements of the optical design. The cut outs, shown on Figure 50, have the function of minimising

the total weight, which is 602 kg. Figure 50 also shows the limb brackets attached to the 'legs' of the tower. The transformer limb is not shown on the figure.

The tower consists of three long plates referred to as 'legs' due to their shape and on top of them there is a platform where the optical assembly sits (see Figure 50). The three vertical plates which are separated from each other are all braced together by a total of three shear panels with triangular cut outs at both sides. The bottom ends of the two longest legs are each supported by two thick plates referred to as the 'feet'. The 'feet' have the function of keeping the tower in a standing position whilst being held with the lifting gear during either installation or removal. Each of the three legs have a total of 24 M8 studs and nuts. The first 20 studs are used to attach the front and back shear panels to the legs as well as the top mounting platform. In addition, a series of thin side plates for reinforcing the edges of the GRP plates to prevent bursting where the studs are located and stiffening the joints were also bolted down with M8 fasteners. There are in total three pairs of side plates for each leg. These pairs form a sandwich with the leg on the front, rear and top as you look at the different sides of the tower assembly. The side plates are only 40 mm wide and 6 mm thickness. The length varies depending on which side and leg they are fitted to. The side plates have the function of compressing the legs, thus preventing bursting of the GRP and improving structural integrity. The side plates are bonded to the leg with epoxy and bolts. The number of bolts along the side plates is two per M8 stud and they are place on both sides of each of the studs on the leg with the exception of the studs for attaching the feet, which perform no function in service. The two rear shear panels with cut outs (see Figure 50) consists of two plates such that one edge sits on top of the other one. These panels held the function of preventing the legs from bending. A two-part construction was necessary for the rear shear panel because it was larger than the available GRP sheet size. Regarding the materials, the tower is made of two types of GRP. The two types of materials are shown in Figure 50. The legs, shown in green colour are made of Durostone® EPC203 (see [27]), and the rest of the GRP plates which are shown in yellow are made of Durostone® EPM203 (see [28]). The reason to change the material for the legs to EPC203 was due to the leg dimensions (*i.e.* it was not possible to fabricate the legs using the EPM203). However, the disadvantage of using EPC203 (see [27]) is that it is necessary to consider the direction of the weave in the fabrication of the sheet, because this affects the strength of the material. Here, one weave direction was designed to align with the primary stress path. By contrast, EPM203 has random fibre orientation in the matrix and the properties are essentially isotropic, which made it the material of choice wherever possible.

The engineering analysis for the tower has been divided into two parts. The first part includes the main results about static stress levels and deformations (see [30]) and the second part has a summary of the harmonic analysis due to ERFA kicks (see [35]). The optical cage was included in the model but only represented as a point mass on top of the tower. The limb is not shown or the limb brackets with the exception of the T-bracket webs. This is because the deformation of the steel is negligible in comparison with the GRP since the limb brackets have a Young's Modulus which is 10 times larger than the GRP. Therefore, it is sufficient to apply fixed boundaries at the T-bracket webs from the limb brackets which are bolted to legs of the tower. The tower was then modelled as a single solid combined with the T-bracket webs into a single part. The unit of length of the mesh used for the calculations is 12.5 mm. The results obtained were that the maximum stress level and associated deformation in the GRP components are 3 MPa and 0.7 mm respectively. The maximum stress of 11 MPa in the steel T-bracket web is an unrealistic 'hot-spot' but is nonetheless still small. The corresponding deformation of up to 0.7 mm is permanent once the whole structure is installed and therefore it is not considered critical for the optical performance. The fixings used for the front and back panels bracing the three legs are also considered acceptable. They are considered secondary connections (see Figure 51 and [31]).

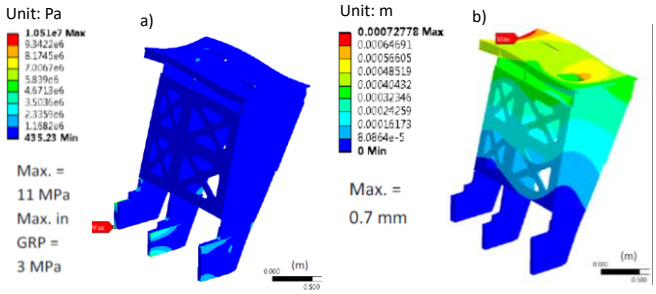

Figure 51 Static stress levels as a function of colour (left or a) and position and associated deformation (right or b).

The second part of the analysis is the harmonic response of the tower due to ERFA kicks (see Figure 52 and [35]). This part of the analysis includes modelling the effect of the optical cage installed on top. Two models were considered, referred to as 'Model 1' and 'Model 2' the difference between them was in how the optical cage was treated: either as a block with the same stiffness as aluminium or as a point mass. Both models assume a damping level of 5%. At the time the analysis was carried out, the weight of the optical cage had increased slightly but the conclusions from the analysis are still considered representative for the current design. The maximum vibration amplitude in metres is plotted against frequency in Figure 52. Each model predicts a slightly different value of the frequency for the different modes represented by the peaks in both graphs. The maximum vibration amplitude for the frequency range analysed is of the order of 1 micron for 'Model 1' and 10 microns for 'Model 2'. The highest peak in each graph is associated with the worst

case of vibration mode of the structure. It is an order of magnitude higher for 'Model 1' with respect to 'Model 2' for the same mode. The author justifies the increase in amplitude from the mode associated to the worst case of vibration with respect to other modes because this mode has a significant level of toroidal rotation that couples well with the ERFA excitation. The excitation would lead to distortion which would affect especially the 'Mounting Plate'. The rotation has been translated into camera pixels - the maximum impact measured in terms of camera pixels is ±0.5 pixels. Finally, a third approach to perform the harmonic analysis consisted of including explicitly the actual base of the frame of the optical cage attached to the mounting plate at the top of the tower and with the rest of the optical cage simplified as a point mass. The level of maximum deformation was similar to the one from 'Model 2'. This deformed shape with maximum deformation amplitude of 0.005 mm translates into ±0.3 camera pixels when the rotation of the base of the frame of the optical cage is considered and it is produced by the mode associated to the highest peak. Summarising all the results presented in this section, the results obtained for both the static analysis and the harmonic response demonstrate that the design is within the technical requirements and thus, fit for purpose (see [35]).

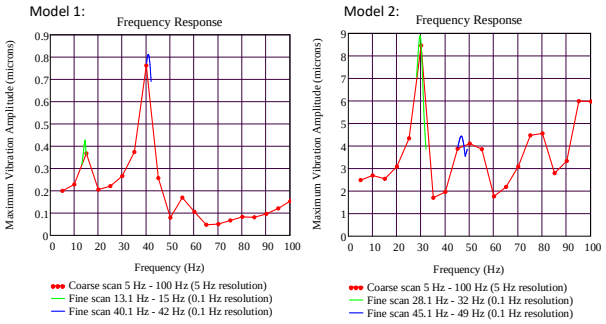

Figure 52 Frequency response of Tower + Optical Cage due to ERFA kicks for the two models

6.2.3 Limb Brackets

The limb brackets are holding the M2&M4 tower to the transformer limb. There are three of them and they are referred to as: 'LH Limb Bracket', 'Middle Limb Bracket' and 'RH Limb Bracket'. The three brackets have a total mass of 250 kg. The material is stainless steel 316L. The shape of the limb fixings is multiform. The main reasons behind this are the same as for the limb brackets for the WAV-M1&M3 assembly: adapt the shape of the bracket to the space available on the limb and secondly, reduce the amount of material to keep only the minimum necessary weight. The shapes and key dimensions are shown in Figure 53. All three of the limb brackets use limb fixing plates with thickness of 45 mm and the thickness of the perpendicular plates are 35 mm.

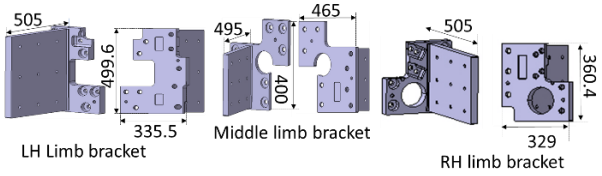

Figure 53 Front and back of the three pairs of limb brackets for WAV-M2&M4 referred to as 'LH', 'Middle' and 'RH'. Dimensions in millimetres.

Each limb bracket consists of two plates positioned perpendicular to each other (*i.e.* T-bracket flange and T-bracket web): the plate with the cut-outs (*i.e.* T-bracket flange) is the one fixed to the limb and the perpendicular one provides the connection to the tower or mounting platform. The drilling of the holes on the brackets was performed after the welding was completed in order to ensure that the welding process did not prevent achieving the required accuracy of all the hole's positions. The fixings size is M20. For all the brackets there are two pin dowels in each bracket on the plate which is attached to the limb to aid with the re-alignment if it has to be removed and refitted.

The details on the engineering analysis for the M2&M4 limb brackets can be found in [31]. The analysis covers first the static von-Mises stress levels and static deformation of the 'T-bracket flange' using finite element analysis. The von-Mises stress levels and static deformation values have been derived from the forces and moments calculated for the mounting tower. The calculation does not take into account the limb itself in order to make the analysis more conservative and treat each of the T-bracket flanges in isolation. Each fixing bolt position is modelled as a single fixed vertex on the face that represents the limb side. However, this produces large 'hot-spot' stresses at the fixations which can be neglected because they are not physical. The realistic maximum level of von-Mises stress found was ~30 MPa which is considered acceptable. The associated static deformation was 0.27 mm. The weld joint in between the T-bracket flange and the T-bracket web for each of the limb brackets was analysed by two different methods: analytical method which considered the three limb brackets as effectively one to which the overall loads are applied and calculated the associated reserve factor and also by a second method using ANSYS where each limb bracket is treated separately with separate loads. All the reserve factors were above 3 which means it is considered fit for purpose.

7. Mechanical Design of the Mirror Relay and Camera systems outside the Torus Hall

Three labs were built in the building adjacent to the Torus Hall (known as 'J1F') to accommodate the viewing systems.

The main requirement for the mechanical design is also to ensure that they were sufficiently rigid to maintain the alignment and at the same time being accessible to the

different imaging optics and camera systems. The labs are constructed on top of each other taking advantage of the available empty space between the lift shaft and the Torus Hall wall. These three labs are referred to as 'Upper Lab', 'Middle Lab' and 'Lower Lab'. The 'Upper Lab' is dedicated to the electrical instrumentation related to the control, data and power signals of the viewing systems. The 'Middle Lab' is the one that houses the two penetrations. This section will describe the main assemblies: Mirrors 5 and 6 of the WAV mirror relay and the mounting of the camera systems.

There is an aperture of approximately 1 m × 0.4 m which connects optically the 'Middle Lab' with the 'Lower Lab' to maximise the allocation of space to the different camera systems in the vertical direction. The 'Lower Lab' is the area for the wide angle infrared camera system (*i.e.* KLDT-E5WC). The mounting of all the camera systems is explained in section 7.1, 7.2 and 7.3.

Finally, a significant advantage of designing the mounting or position of the viewing systems outside the TH is that there is no constraint on the type of material to be used due to any loads driven by electromagnetic fields or concerns of effects caused by radiation. As an example, aluminium alloy is used for all the bracketry.

7.1 WAV Mirror Relay outside the Torus Hall

The last two mirrors of the mirror relay are located outside the Torus Hall - these are M5 and M6. Figure 54 shows the side and top view of both mirror assemblies. In addition, the arrows (left hand side) depict the sequence of the light path. The M5 and M6 mirror assemblies are fixed to the concrete TH wall using resin-bonded anchors. Each assembly will be described separately in sections 7.1.1 and 7.1.2.

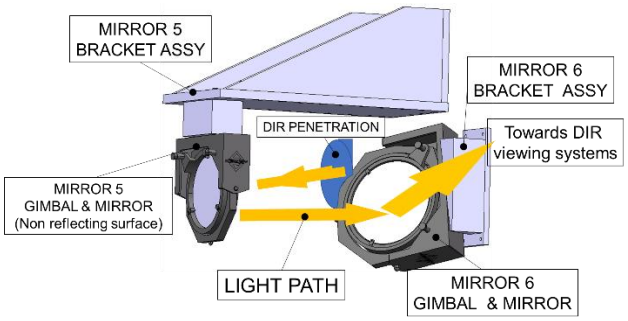

Figure 54 Side and top views of the M5 and M6 mirror assemblies.

7.1.1 WAV M5 Assembly

The M5 assembly can be subdivided in two main components: the gimbal mount and the mounting bracket. The dimensions of the M5 bracket sub-assemblies (*i.e.* without the gimbal mount and mirror) are shown in Figure 55 for their key mounting components respectively.

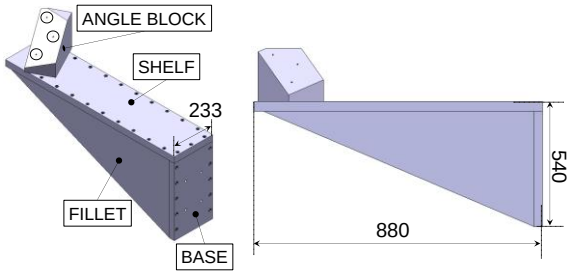

Figure 55 Key components and dimensions in millimetres of M5.

The M5 bracket assembly weighs 46.3 kg and it consists of the following components: 'Angle Block', 'Shelf', 'Base' and 'Fillet'. The function of the 'Angle Block' is to position the M5 mirror at the approximate angle to receive the reflected light from mirror M4 within the Torus Hall and reflect it to M6. The three holes in the form of a triangle on the top face of the 'Angle Block' align with the holes of the base of the gimbal mirror mount (these holes have been highlighted in the figure). The overall dimensions of the 'Angle Block' are 200 mm × 120 mm ×160 mm and it weighs 6.9 kg. The dimensions of the bracket sub-assembly are 880 mm × 200 mm × 30 mm. The 'Base' is the side which attaches to the outside of the biological shield wall using four holes in the central section of the component. Finally, the 'Fillet' has a triangular shape to minimise the weight of the complete M5 assembly. The fasteners size to join all the plates is M8.

An off the shelf gimbal mount from Aerotech with model number A0M110-10 (see [26]) is used to hold the mirror M5. Three tabs placed separated by 120º around the mirror press against the mirror to retain it in the inner gimbal ring. Each tab is attached to the inner ring by a button head screw with a flat nylon tipped grub screw for contact with the mirror surface.

7.1.2 WAV M6 Assembly

The last mirror assembly within the mirror relay is M6 (see Figure 54). The key dimensions and components are reported in Figure 56. The complete assembly weighs 45.7 kg. The concept is similar to M5. The 'Angle Block' is used for holding the gimbal mirror mount in the correct position provided by the optical design. It weighs 16.7 kg with dimensions 350 mm × 130 mm × 168.5 mm.

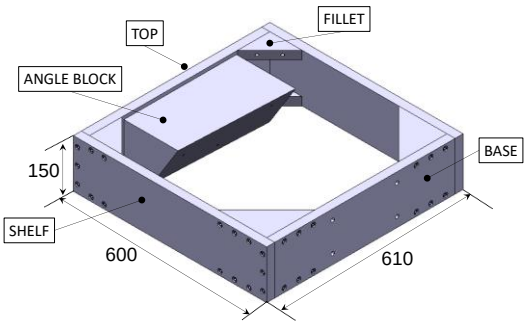

Figure 56 Key components and dimensions in millimetres of M6.

The plates forming the rectangular shape are strengthened with the use of 'Fillets'. Fixing sizes are M8 and M12.

The M6 gimbal mirror mount is larger than M5 with dimensions 463.4 mm × 494.4 mm ×154 mm. However, it is also an off-the-shelf from Aerotech with model AOM110-12 (see [26]).

7.2 Mounting of WAV camera systems

The camera systems share the 'Middle' and 'Lower' labs (see Figure 57).

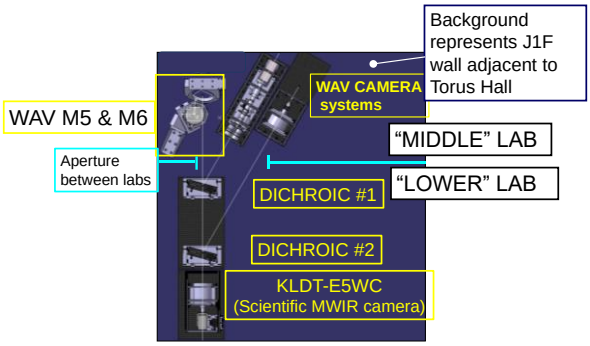

Figure 57 Schematic of WAV camera systems in the Middle and Lower Lab.

The basic concept for the engineering design is that the cameras are housed inside a supporting frame and mounted onto an optical breadboard, which, in turn, is fixed to the wall. Thus, the camera systems 'hang' vertically from the side outside the biological shield wall. In the 'Middle Lab' there are two optical breadboards as shown in Figure 58, one for the cluster of visible cameras and a slightly wider one for the protection camera. The two optical breadboards are made of aluminium alloy, they are also anodised with a matt finish. The optical breadboard dimensions for the cluster of visible cameras are 1200 mm × 400 mm. Secondly, the optical breadboard dimensions for the protection camera are 1200 mm × 450 mm. M6 is the hole size for both optical breadboards. The optical breadboards were supplied by Thorlabs (https://www.thorlabs.com/). Figure 58 provides a front view of the camera systems inside the 'Middle' lab. The top mounting frame consists of strut profiles with 8 mm channels of several length sizes (330 mm, 350 mm, 390 mm, 1190 mm) but keeping the same cross-sectional size as 30 mm × 30 mm. There is a total of 32 strut profile parts. A long flat plate is used as a base platform for attaching the three camera devices. Its dimensions are 935 mm × 250 mm × 12 mm. In addition, it uses × 12 M6 size holes and × 16 M8 size holes. There are also some brackets to clamp the optical lenses to the base plate. This figure also shows the triangular packing of the visible cameras as mentioned in section 5.3.

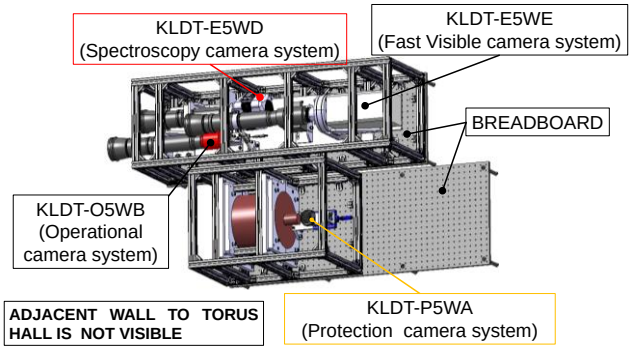

Figure 58 Overview of the WAV camera systems in the 'Middle' lab.

As seen in Figure 58, the protection camera is mounted in a separate supporting frame (see Figure 59). It consists of the strut profiles forming the outside frame and plates of the clamping lens assembly. The overall dimensions are 630 mm × 430 mm × 440 mm. The enclosure is formed of 24 strut profile parts of 8 mm channel size and cross-sectional size 30 mm × 30mm with different lengths (180 mm, 370 mm, 380 mm and 630 mm). The clamping lens assembly is shown in Figure 59. This is used for holding the telescope. There are two sets of clamping plates which are mounted along the enclosure length. Each set of plates is a combination of a rectangular plate and two semi-circular plates that clamp around the body of the optical housing. The dimensions of the rectangular plates are 340 mm × 350 mm × 20 mm. On the front side there are four recessed spots which have been introduced to insert four short strut profile parts to prevent the plates from separating or tilting and thus, increase stiffness.

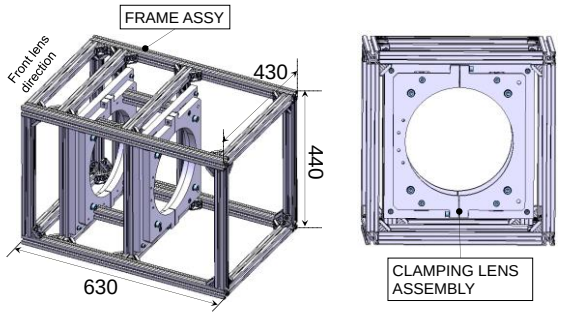

Figure 59 Mounting frame for the holding the telescope of the protection camera (KLDT-P5WA).

The fixings are size M8. There is an additional bracket sub-assembly called 'Swivel Bracket assembly' (see Figure 60). This whole bracket is bolted onto one of the semi-circular plates from the lens clamping section. The translation stage enables the adjustment of the focus position by allowing the camera to move along its optical axis with respect to the telescope. It is referred to as the 'Swivel Bracket' because it enables the rotation of the camera to optimize the orientation of the sensor shape with the field of view.

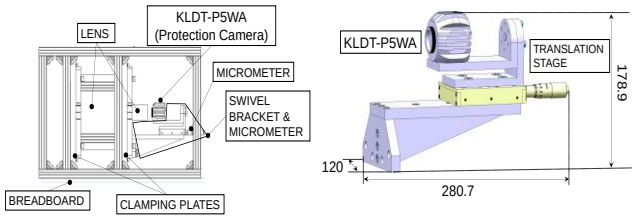

Figure 60 Detail of mounting of the protection camera.

Although M6 is the last assembly of the WAV mirror relay, it is not the final component of the common relay optical system. The light reflected from M6 is directed to the pair of dichroics (see section 5 and Figure 57 as well as Figure 61).

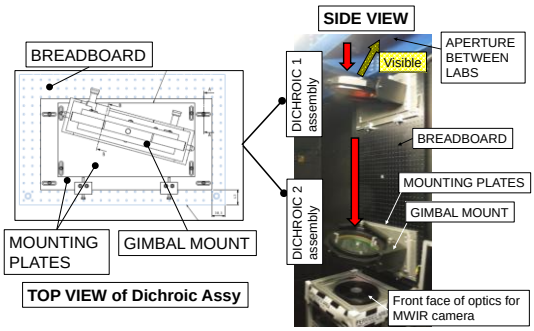

Figure 61 Side view of dichroic pair in the 'Lower' lab.

The two dichroics are necessary to reflect the visible wavelength range from the first (top) dichroic and the near infrared wavelength range by the second (bottom) dichroic, thus transmitting only the wavelengths in the middle infrared wavelength range to the scientific camera below. The pair of dichroics and the enclosure for the scientific mid-infrared camera and its telescope are mounted vertically onto a third optical breadboard which, in turn, is also attached to the outside wall of the biological shield wall. The diameter of the dichroics is 250 mm. They are held by gimbal mounts from Aerotech (model AOM110-10). The gimbal mounts are fixed onto a top plate that enables the gimbal to slide vertically and a bottom plate which enables the gimbal to move horizontally, for ease of initial coarse positional adjustment. Both dichroics are positioned at an angle of incidence of 15º to the light path for alignment purposes with the camera systems sitting above in the 'Middle' lab.

The enclosure frame of the scientific mid-infrared wide angle view camera (KLDT-E5WC) is mounted as shown in Figure 62.

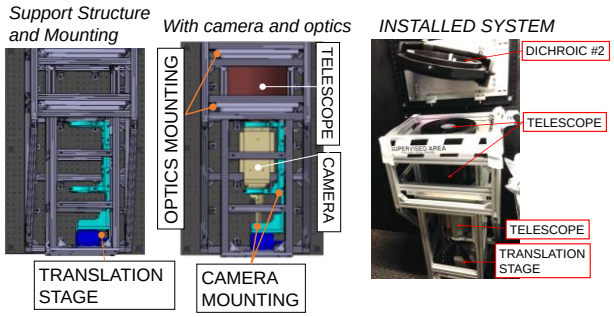

Figure 62 Front view of the enclosure on its own (left), the enclosure with the camera and telescope (middle) and a photo only including the bottom dichroic and the front end of the telescope (right).

The overall dimensions are 902 mm × 410 mm × 460.1mm. This frame is modular with the same strut profile design as the ones previously described. There is also a pair of clamping plates to hold the telescope and an additional bracket with a translation stage attached to it enabling the adjustment of the focal position by moving the camera vertically along its optical axis relative to the telescope. The camera is held by circular clamps such that it is possible to set the orientation to optimise the sensor shape to the field of view.

8. Penetrations through the Biological Shield Wall

The penetration through the biological shield wall enables the transmission of the light path from the Torus Hall towards the cameras housed in the adjacent building. Although, two penetrations were constructed, one for each line of sight respectively (*i.e.* WAV and a separate system for viewing the divertor named Divertor Infrared (DIR) detailed elsewhere (see [37]), this section focuses on the penetration for the WAV line of sight but the design considerations are the same for DIR. Figure 63 is a diagram showing the WAV and DIR penetrations.

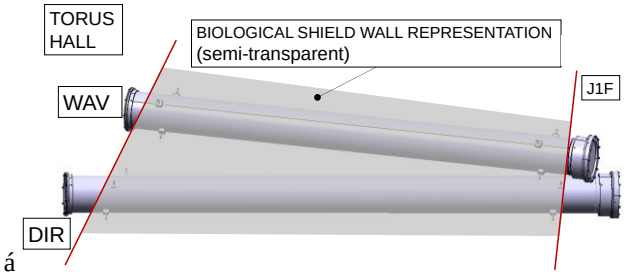

Figure 63 Schematic showing two penetrations for the WAV and DIR line of sights.

The overall dimensions and key features are given in Figure 64. The tube end inside the TH is open, whereas a window housing is present at the end outside the TH. The key components are: 'Tube Assembly', 'Window Housing',

'Gasket' and 'Alignment Adjusters'. The window as an optical component has been described in section 5.

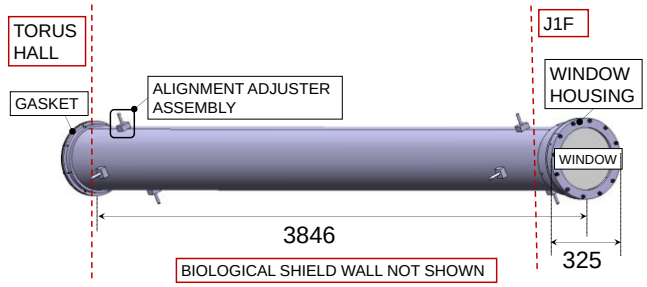

Figure 64 Schematic of the WAV penetration.

The complete 'Window Housing' sub-assembly is presented in Figure 65. The 'Window Housing' is a flange with a height of 95 mm and a diameter of 325 mm. There are channels inside fitted with O-rings to make a seal between the TH and lab environments. The tube's material is stainless of 1.4301 (314) grade. It weighs 9.1 kg. There are two types of O-rings, they have been represented in orange colour (see Figure 65). The one closest to the window has a diameter of 8 mm and a length of 262 mm. This O-ring has the function of sealing the window within the window housing. The second one has a diameter of 5.7 mm and a length of 269.3 mm. Its function is sealing the window housing over the tube. The 'Window Housing Cap' captures the window inside the 'Window Housing'. The fixings size is M8.

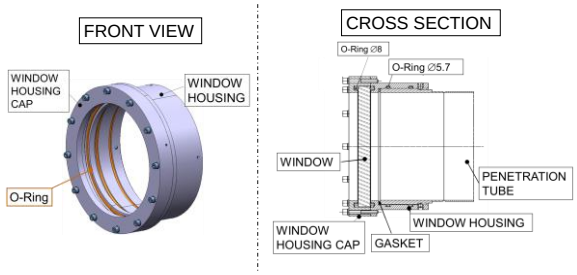

*Figure 65 Front view and cross section of the penetration end **outside** the Torus Hall.*

The penetration end inside the TH is shown in Figure 65 and consists of three components: 'Aperture Ring', 'Aperture Clamp Ring' and 'Aperture Shield'. Some of the key dimensions such as the outer diameter of 300 mm and the inner aperture of 182 mm are listed in Figure 66. In addition, a cross-sectional view showing the fixings has been included. There is a total of twelve M6 x16 mm hex. Socket cap head screws and M6 washers. The 'Aperture Shield' is held onto the penetration tube end by the 'Aperture Ring'.

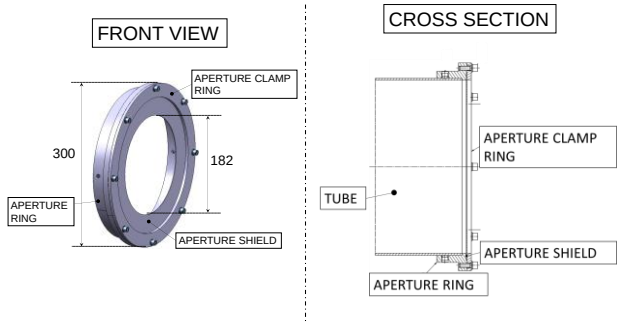

Figure 66 Front view of the 'Aperture Ring' assembly which is located inside the Torus Hall.

The first stage of the installation of the penetration tubes was the drilling through the biological shield wall. This was undertaken by an in-house team hiring specialist drill equipment since radiation activity and contamination levels of the biological shield wall were confirmed as negligible. In order to minimise the potential disruptions to operations, the drilling started from the outside of the TH. A pilot hole through the biological shield wall was produced first. The pilot hole was also used to check the positioning for the penetrations by referencing from outside to inside the TH. This activity started before the construction of the labs housing the camera systems. The holes drilled for each of the two penetrations had a diameter of 400 mm. Once the drilling was completed, the next stage was the installation of the penetration tubes. The installation of the tubes could only be done from the TH side due to the length of the tubes and it had to take place during a non-operational day. As a result, a blanking plate had to be fixed to the wall in the meantime. The lifting and transportation of the penetration tubes was carried out using the main crane and holding the tubes with lifting slings (see Figure 67 (left side)). The method for aligning the penetration tubes was to use a number of 'alignment adjusters' (see Figure 64). The concept of the adjuster was to use four M12 screws (nominally 110 mm long but interchangeable when adjusting if needed) threaded through adjustment blocks, which were welded to the tubes at each end, to control the stand-off position from the inside of the drilled hole in two axes (see right side of Figure 67). This allowed each end of the tubes to be set to the axis of an alignment laser for each line of sight which co-aligned the tubes on the respective axes ready for them to be cast into the wall. The adjustment screws also held the tubes in position before the grout filling was set.

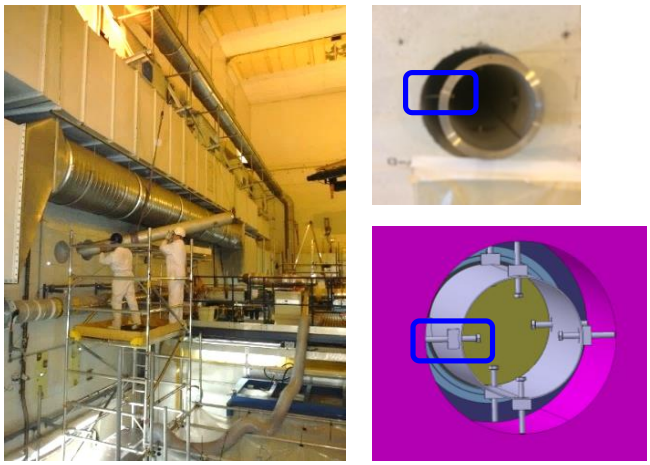

Figure 67 Left: Photo taken during the installation of the WAV penetration tube. Right: Photo and model of the alignment adjusters used during the alignment of the penetration tube.

Once the penetration tubes were installed and aligned, the annulus around the penetration tubes was filled with a high-density grout. The set grout was specified to reach a density value of 2800 kg/m^3. The next two photos (see Figure 68) present the WAV and DIR penetrations on both sides (*i.e.* outside and inside the TH respectively).

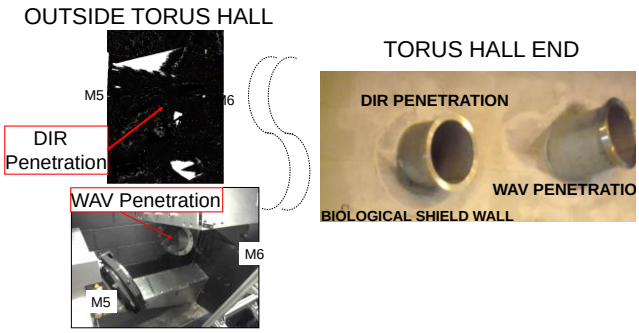

Figure 68 Left: Penetration tubes end outside (left) and inside (right) of the Torus Hall for both WAV and DIR lines of sight.

9. Radiation Shielding

The opening of the penetrations presented a safety risk in terms of radiation leaking outside the Torus Hall. This section will discuss the radiation shielding for both lines of sight rather than focus only on WAV due to the proximity of the two penetrations (WAV and DIR) including sharing the same lab (*i.e.* 'Middle Lab'). A neutronics analysis was carried out (see [38]). Table 11 summarises the key results from the neutronics modelling. The number of neutrons expected for the three different pulse types (*i.e.* DD, DTE1 and DTE2) indicates that the radiation dose significantly exceeds the threshold for DTE2 and therefore shielding is required for the neutron flux exiting the TH through each of the penetrations.

	DD Pulse	**DTE1 Pulse**	**DTE2**
Number of neutrons	1.25e+17	2.5E+18	1.7e+21
Threshold (µSv)	10.00	10.00	1,000.00
Dose in front of shield (µSv)	1.14	22.84	15,530.20
Dose Behind shield (µSv)	0.03	0.64	435.16

Table 11 Neutrons and dose as a function of fuel type.

The shielding consists of a series of blocks made of polyethylene with steel plates in between. The overall dimensions are 260.5 mm × 506 mm × 25 mm. The individual polyethylene block is 50 mm thick, and the steel plate is 5 mm thick. In addition, the wall panels directly behind the shielding blocks have only polyethylene (*i.e.* no steel plate in between). Figure 69 provides a model of an empty 'Middle Lab' showing only the location of the shielding blocks for each of the two lines of sight. The wall which appears coloured in green is the one that has the polyethylene panels (see Figure 69). The installation of the polyethylene slabs in the wall also prevented people travelling in the lift behind from being exposed to unsafe levels of neutron radiation.

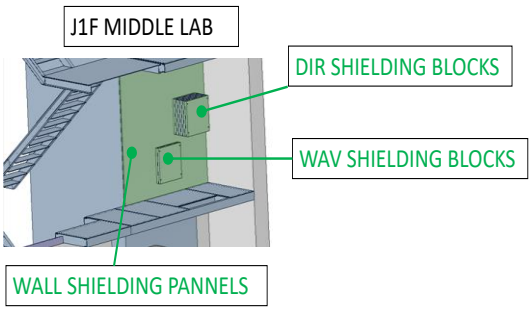

Figure 69 Schematic of the shielding blocks for both lines of sight.

The WAV penetration only requires two sets of polyethylene blocks with the steel plate whereas the DIR penetration requires more shielding blocks because the orientation of the DIR penetration points directly at the plasma position in the TH whereas the WAV penetration axis points above the machine (see Figure 70).

Figure 70 DIR shielding blocks.

10. Operational Experience

This section assesses the performance of the WAV line of sight based on the experience gained through JET operations since the installation was carried out in 2017. The main outcome is that the overall performance has been considered very successful and this has been reflected in the significant role that the protection camera played during the recent campaign of D-T experiments and the valuable data for the different experiments provided by the scientific camera systems. However, there has been one particular issue related to excessive image movement which will be described in this section as well as the corrective actions taken to resolve it.

The protection camera is required to be able to calculate accurately the surface temperature of the plasma facing components. This, in turn, requires an image quality which can resolve spatially and temporally the tiles within the field of view. Image shaking carries the potential to invalidate the temperature measurement by decreasing the quality of the images in both regards. During the design phase, the potential for image movement was investigated and as a result a target was set of ±1 pixel of movement for the protection camera system. Pixel here means pixel size of the protection camera (*i.e.* KLDT-P5WA) which is 15 µm for the camera used for this function but was originally 30 µm by design. The only exception to this requirement was that it did not apply during a disruption. The reason being that during a disruption the signal saturates due to the plasma losing its confinement and radiating towards the walls of the vessel.

After the WAV system was installed, excessive image movement became noticeable on the operations viewing camera (*i.e.* KLDT-O5WB), manifesting as blurring during certain pulses. The level of blurring could vary for different experiments such that it was only minor for some but then rather severe for those experiments which utilise ERFA 'kicks'. The 'kicks' are magnetic field perturbations used to generate rapid vertical movement of the plasma as previously described (see [33]). The amplitude of the image movement was measured using the mid-infrared wavelength camera (KLDT-E5WC) due to its higher temporal resolution (~2 kHz) in comparison with the protection camera (25 Hz). The results yielded a range of between a few pixels of movement peak to peak to a worst case scenario of 60 pixels peak to peak during plasma kicks for a particular range of frequencies.

A separate team was charged with the task of identifying first the root cause and following from that a solution. The root cause was found to be due to rapid perturbations of some of the mirrors within the relay, caused by resonant excitation from eddy current loads acting on the metallic gimbal mounts and the mounting not being sufficiently rigid to mitigate these deformations and movements. Initially, this was identified by gentle tapping of the mirrors within the mirror relay inside the TH. This established the resonant frequencies of the different mirrors and comparison with experimental data then showed which specific mirrors were contributing significantly to the problem. From the tapping exercises, three mirrors were identified to be susceptible: M1, M3 and M4. Note that the largest mirror, M2, was not believed to be a source of significant vibration, thus vindicating the decision to design a bespoke GRP mount for this mirror. With hindsight, bespoke GRP mounts for all the mirrors would probably have prevented the problem. However, at the design stage there was a preference to use off-the-shelf mirror mounts wherever possible, since design of novel GRP mounts carried additional risk and cost. Alternative solutions considered were to modify off-the-shelf mirror mounts to insert insulating breaks in the gimbal rings or to use stainless steel mounts, but these were unorthodox solutions and not without further unique risks. Operational experience, however, has proved the success of the GRP mirror mounts, which may benefit future fusion devices. A sensitivity analysis was carried out for the three mirrors of concern (see Table 12, [39]). A comparison of the ERFA torque (without resonant amplification), relative torsional stiffness and angular sensitivity was calculated for the three mirrors, and it was determined that M3 (also the one with the largest diameter mirror after M2) was exercising the highest impact on the level of deflections, followed by M1, whereas the M4 mirror played only a relatively minor role in contributing to this type of behaviour.

Mirror	ERFA torque (Nm)	Relative Torsional Stiffness	Relative Angular sensitivity	Relative Impact
M1	0.7	0.23	0.51	0.64
M3	2.4	1	1	1
M4	0.3	0.70	0.21	0.04

Table 12 Sensitivity analysis of three WAV mirrors.

There were however, two main constraints in identifying a solution. Firstly, the mirror assemblies could not be dismantled and modified since this would invalidate the calibration of some of the camera systems. The protection cameras and the scientific ones operating in the mid-wavelength infrared had an absolute calibration obtained by using a hot source inside the vessel. This type of calibration can only be performed during a long period of shutdown which was not part of the programme for another couple of years. Consequently, the solution had to lay in increasing the stiffness of the current mounting by retrofitting additional supports to the existing ones. The two mirror assemblies that were fitted with additional supports were M1 and M3. Both retrofitting assemblies are modular as this was the only way to install them into the existing supports.

Secondly, the performance of the camera system installed originally on the endoscope had also been measured separately (*i.e.* before the two lines of sights were designed) and it was found that image movement was significantly less than ±1 pixel but on the other hand it was not zero either, with certain

pulses suffering worse than others. Since the in-vessel mirror box and endoscope was already part of the WAV line of sight, any improvement to the mitigation of image movement already had the contribution of these two components as a baseline.

The potential for resonant vibration of the mirror mounts during ERFA kicks had been identified at the design stage, and a detailed engineering analysis performed to demonstrate that the associated image movement would be acceptable. A forensic re-examination of this analysis did not reveal any single factor that led to the erroneous conclusion. Rather, it is believed that the assumptions made in determining magnetic field conditions, resulting eddy current loads and associated mirror mount deformations and movements with resonant amplification combined unfavourably. For example, values of mechanical damping specified in design codes for seismic analysis and adopted in the original analysis are typically too high for the analysis of resonant behaviour with small amplitude. This was demonstrated by the mirror 'tap tests' and discovered in a subsequent search of the scientific literature (see [40]). It is important to note that radial field pulses are also used in general feedback control of plasma vertical position and stability. There are situations other than ERFA kicks where this control function leads to pulses of nearly constant frequency, e.g., in response to ELMs as opposed to triggering ELMs. These situations can also cause vibration and excite resonances in mechanical assemblies, although operational experience has shown their effects to be generally less severe than those of ERFA kicks. Designers should carefully consider any sources of periodic excitation, including power supply switching frequencies, when designing sensitive optical relays

10.1 Additional supports for WAV-M1

An exo-skeleton clamping the M1 gimbal mount inner ring was installed to mitigate the mirror deformations and movements. Figure 71 presents a model of the exoskeleton showing the key components. The overall reference dimensions are 342.06 mm × 250.76 mm × 234.5 mm. The weight is around 5.4 kg. The components made from GRP are shown in a brown colour. GRP offers the advantage that it eliminates the possibility of current loops in between metal parts.

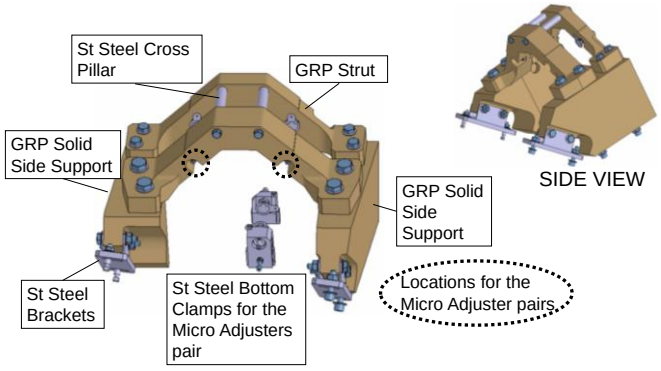

Figure 71 Exoskeleton model for M1 mirror showing the key components.

This exoskeleton consists of two struts following the shape of the gimbal mount and two side supports (see Figure 71). The two GRP struts were connected to two stainless steel pillars. In turn, the struts are fixed to the side supports using M6 Helicoils and M6 hex head screws together with wide flat washers to spread the load. Secondly, each of the GRP side supports were fitted to stainless steel brackets, which, in turn, were fitted to the base plate of the M1 sub-assembly. The fixings in between the brackets and the GRP side supports were originally designed as M8 size. However, due to an undocumented offset on the as-installed position of the base plate, it was changed to mainly using M4 size.

Figure 72 shows photos of the M1assembly before and after the new exoskeleton was installed. The top photos show the M1 sub-assembly and photos below provide the context of its location inside the 'Optical Cage' (see section 6.1.1 and Figure 27 and Figure 28). Due to space constraints, it is not possible to show a clear photo of the assembly and instead two models have been included presenting a side and front view of the M1 gimbal and the exoskeleton.

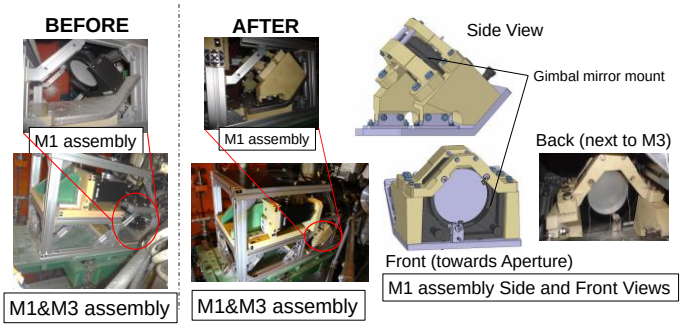

Figure 72 Before and after retrofitting exoskeleton for M1 mirror.

Finally, there are three pairs of micro adjusters, each pair positioned equidistant from the other two (not shown on Figure 72). These pairs were mounted such that they apply pressure from opposite sides of the gimbal mirror mount's inner ring in three locations in order to controllably secure the inner ring but without inadvertently causing distortion or

misalignment of the mount or the mirror when fitting. These micro adjusters were supplied by Newport (https://www.newport.com/). The model number is BH30.10 with a sensitivity of 1.4 µm and a travel range of 10 mm. The maximum load is 408 N. The micro adjusters tips contact the mounts using additional stainless steel 'cups' which spread the loads to prevent puncturing the gimbal's anodised surface. In addition, they can be locked in position using a 3 mm Allen key. Engineering analysis was undertaken to ensure that the maximum load rating of the micro-adjusters would not be exceeded in service, either during pre-loading of the clamps, ERFA kicks or a worst-case plasma disruption. The associated maximum stress and deformation of the GRP components of the additional supports were predicted to be small: 4 MPa and 23 µm respectively (see [42] and [42]).

The additional supports fitted to the M1 gimbal mount give two benefits in relation to mitigating potential vibration during ERFA kicks. Firstly, the static stiffness is increased and, secondly, the natural frequencies of the M1 assembly are increased as a result of the additional stiffness, to the point that they are beyond the frequencies of concern for ERFA kicks. The dynamic amplification factor that had been occurring as a result of resonance is thus reduced. Note that the rectangular pulse nature of the ERFA kicks means that their energy may be spread over a wide range of harmonics, so the frequencies of concern had to be identified from operational experience and were $\lesssim$ 150 Hz. Note also that the amplitudes of relevant individual harmonics relative to the overall pulse amplitude must be considered when evaluating dynamic amplification. Modal analysis predicted that the additional supports increased the first natural frequency of the M1 assembly from ~140 Hz to ~500 Hz. Hence, the frequencies of concern for ERFA kicks now fall well within the 'tail' of the response associated with the first natural frequency, effectively eliminating dynamic amplification completely. The first natural frequencies measured in the tap tests on the M1 assembly without the additional supports were ~110 Hz, 120 Hz and 140 Hz, *i.e.* a 'triplet' of natural frequencies where the analysis predicted only one. This is thought to result from subtle details of the assembly structure and structure interfaces that were not captured by the model but, nonetheless, the tap tests gave some confidence in the model predictions. The analysis predicted that the combined effect of increased stiffness and elimination of dynamic amplification from the additional supports would result in a reduction of image movement during ERFA kicks by a factor of ~200 (see [43]).

10.2 Additional supports for WAV-M3

The WAV-M3 sub-assembly is a cantilever type where the gimbal mount is positioned horizontally, and its base is attached to a supporting GRP bracket (see Figure 28). The role of the additional supports is to clamp the inner gimbal ring and, in particular, to mitigate the deflection of the mirror's end furthest away from the mounting bracket. This was achieved by installing a support arm as represented in Figure 73. The overall dimensions are 512.37 mm × 313.41 mm × 323.86 mm. The brown colour in Figure 73 represents the GRP material.

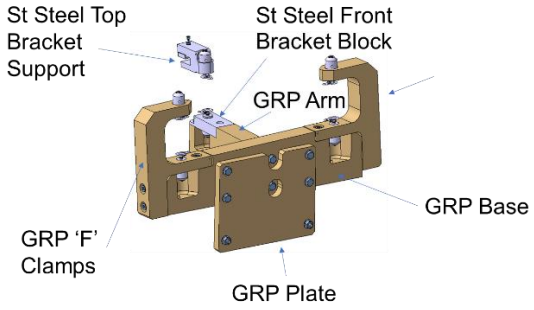

Figure 73 Additional support arm retrofitted into WAV-M3 sub-assembly showing key components.

The two 'F-clamps' are fixed to the 'GRP Base' using M6 Helicoils and M6 cap head screws. The 'GRP Plate' is fixed to the 'GRP Plate' using M8 size Helicoils and cap head screws (see Figure 73). There are three pairs of micro adjusters, two at the front and one at the back. This provides six points of contact between the micro adjusters and the inner gimbal mount ring. The support structure fits between the base of the M3 mounting bracket sub-assembly (see Figure 74) and is secured at the front via a plate (see Figure 73) with two 40 mm T-bolts into the 'Optical Cage' frame structure. The micro adjuster at the back, next to the vertical side of the M3 mounting bracket sub-assembly was fitted into a support bracket and clamped to the gimbal chassis. The micro adjusters within the 'F-clamps' are secured using M20 × 1.0 mm threads.

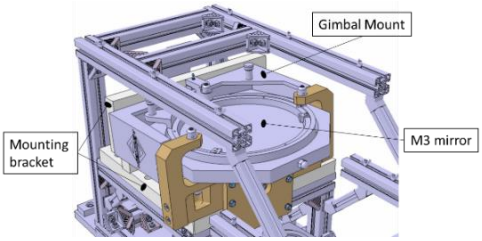

Figure 74 View of the additional support arm within the WAV-M3 sub-assembly.

Engineering analysis was again undertaken to check that the load rating of the micro-adjusters would not be exceeded in-service and that the associated maximum stress and deformation of the GRP components of the additional supports would again be acceptably small.

Modal analysis predicted that the additional supports increased the first natural frequency of the M3 assembly from ~ 60 Hz to ~ 280 Hz, again essentially eliminating dynamic amplification at the frequencies of concern for ERFA kicks. A

similar 'triplet' of natural frequencies as for the M1 case was found in the tap tests, overlapping with the first natural frequency predicted by the analysis, again giving some confidence in the simulations. For M3, the overall reduction in image movement due to the additional supports was predicted to be ~ 100.

Overall, the engineering analysis demonstrates that the improvement of increasing the stiffness in the M1 and M3 gimbal mounts should result in an improvement factor higher than 100. Measurements taken of the image movement after the additional mounting was installed yielded a ±1-2 pixels amplitude (see [44]). The only exception was during plasmas with ERFA kicks at certain frequencies where the amplitude of the image movement could reach ±5 pixels. Although this exceeds the original requirement of ±1 pixel, it is still a huge improvement from the initial experience of ±5 pixels and ±60 pixels for pulses with vertical kicks. It is also recognised that the ±1 pixel requirement was not necessarily realistic as a system requirement given the existing contribution from the in-vessel mirror box and the endoscope. In addition, by enlarging slightly some of the regions of interest within the field of view of the protection cameras and introducing additional checks to the camera signals in the control algorithm it was possible during D-T campaign to overcome the residual image movement. The scientific cameras, such as the wide-angle-view (KLDT-E5WC) and the spectroscopy camera (KLDT-E5WD) were also able to be used as additional video data to identify any potential damage.

Finally, it should also be highlighted that the only operational time lost due to the performance of the camera systems was minimal (less than ~ 1 h in total for the whole of the DT campaign) and it was due to a couple of occasions where either the protection or the operational camera failed to initialise due to a communication issue with their respective computers which could had been also network related.

10.3 Calibration

The readiness for the D-T campaign included the removal of all the camera systems located inside the Torus Hall and around the machine. Consequently, it was necessary to perform an independent calibration of the multiple imaging diagnostics associated to each of the line of sight (*i.e.* WAV and DIR). An absolute calibration requires to take into account all the optical components within the line of sight and therefore this is usually carried out by placing a suitable source inside the vessel. The source is placed and manipulated by the by the JET servo-manipulator (see [30]). There are two different types of sources used for the near infrared protection cameras and the scientific MWIR cameras. The method and procedure which was followed for the production of an absolute calibration of the protection cameras can be found in [45] and for the scientific MWIR cameras in reference [46]. It should be pointed out that the last two references relate to the camera systems prior to the construction of the WAV and DIR lines of sight.

10.4 Commissioning

The goal of the commissioning of the WAV line of sight was to demonstrate the optical performance and functionality of the camera systems. As mentioned earlier, the field of view was the most important parameter since the main goal was to be able to image most of the plasma facing components inside the vessel. The field of view was first confirmed, still during the shutdown, after the completion of the installation and alignment of the WAV mirror relay and its associated camera systems. This was performed using the operational camera (KLDT-O5WB) which operates in the visible range and thus, it made it the easiest choice. The image was obtained using the in-vessel illumination system and confirmed that the field of view met the requirements (see Figure 4). As for the rest of the cameras operating in the visible range, the same check was repeated without using any filters in front of the cameras (see section 4). However, for the protection and scientific cameras operating in the infrared it was not possible to use the same procedure. Instead, it was necessary to wait until resuming JET operations. However, the fact that all the camera systems share the same light path, provided sufficient confidence to enable to proceed with the rest of the commissioning exercise. The images shown in section 4 are proof that the field of view target was also achieved for the cameras operating in the infrared wavelength range. Furthermore, the images obtained also demonstrated that the image quality is sufficient to identify the different plasma facing components.

The second phase of the commissioning carried out during the shutdown was first a functional type. This was specifically related to the validation of all the software tools dedicated to the acquisition and recording of all the camera signals as well as the input of camera settings. This also included the testing of those camera systems which included a filter wheel. Once operations started, there was a second phase for the commissioning which consisted in demonstrating the validity of the recorded images. This was carried out by comparing wherever possible with other JET diagnostics, for example the images produced from the spectroscopy cameras were compared with the spectrometer signals to cross-check that the camera data was meaningful. Furthermore, the temperature measurements obtained from the infrared camera systems were compared between the protection camera systems operating in the near infrared with respect to the values obtained from the mid-infrared camera systems since the calibration of the near infrared and the mid-infrared camera systems was performed using different sources and different procedures. The outcome of the commissioning demonstrated that the camera systems had met the project requirements also from the functional aspect.

10.5 Operational Schedule and Arrangements

Both the protection and scientific cameras for the WAV and DIR line of sights were used daily during the Tritium and D-T campaigns as well as every other campaign since they were installed. The operational schedule, except for the D-T campaign, extends from Monday to Friday generally with two shifts each day. Occasionally, there are also operations during a Saturday with also two shifts. The availability of the protection cameras is essential for the execution of the pulses. There is an operator in the control room, known as the 'Viewing System Operator' (VSO), who is responsible for monitoring the running of the protection cameras and analysis of the images and signals recorded during the pulse. The VSO operator is also responsible for liaising with the 'Engineering in Charge' and the 'Session Leader' during the experimental shift to discuss any observations and inform them of any concerns related to the overheating of the tiles in support of operational decisions. The 'Engineer in Charge' is responsible for the integrity of the JET machine and the safety of personnel. The 'Session Leader' is responsible for the detailed specification, preparation and execution of the session to meet the objectives of the previously agreed programme.

On a weekly basis, the VSO operators meet in a forum to review the comments, observations and (if applicable any alarms) found the previous week. The meeting is carried out via Teams, and it is also used to improve the learning and understanding of the whole VSO team based on the experiences of those VSO operators who were rostered during that week. Furthermore, there is also a separate Teams channel that has the function of posting any questions or comments found during a session to the whole VSO team, so the members are supported during the shifts as much as possible.

Secondly, for the scientific cameras, a similar approach is used. A dedicated Teams channel was set up for posting any questions or comments during the session to all camera operators in order to optimize the level of support provided in each session. Furthermore, ahead of each week, the camera operators prepare a list of settings for the experiments planned during the coming week. During each session, the operators are responsible for refining the initial settings if found necessary for improving the data quality of the recorded videos. During the D-T campaign, the responsibility of operating *any* JET diagnostic (not just the ones described here) was embedded into a new role referred to as 'Rostered Diagnostic Expert' which required for the operator to confirm prior to the start of the pulse the readiness of the diagnostic. The application of this role to the WAV and DIR imaging systems led to the creation of two groups of camera operators to ensure that there was sufficient level of resources to input the set of parameters, confirm the availability of the camera systems as well as carrying out an initial check of the data quality. These two groups were divided as follows: one group was dedicated to the MWIR cameras for both WAV and DIR lines of sight and a second group was only dedicated to the spectroscopy camera (KLDT-E5WD) associated with the WAV line of sight. This meant that two operators were required for each shift. The two-camera operator arrangement proved to be very successful, and it continued after the D-T campaign when during the post D-T intervention, the cameras which were removed before the D-T campaign were subsequently re-installed.

11. Conclusions

A detailed description of a remote wide angle viewing system which includes multiple camera systems and is capable of imaging from outside the Torus Hall using a mirror relay 40 meters in optical length is presented here. It has demonstrated being compatible with Deuterium-Tritium operations. In addition, it encompasses a broad wavelength range, which extends from visible to the middle infrared in order to provide a number of applications which cover the protection of the plasma facing components to the scientific exploitation during the experimental campaign. The specifications of the optical components, camera systems as well as the engineering of the mounting structures are reported together with the reasons behind the key aspects of the design. Furthermore, a novel kinematic mount made from glass reinforced plastic for a relative large mirror of 500 mm is also described. The WAV line of sight has met the overall performance of the protection and scientific camera systems which includes the field of view, spatial and temporal resolutions as well as the temperature ranges for the systems operating in near and middle infrared. Finally, the operational performance of this viewing system has been assesed together with the solutions implemented to mitigate the movement of images. This work provides to designers and operators of future fusion devices useful experience that is currently unique in this field because of the unique set of constraints that come from tritium and D-T operations.

Acknowledgements

This work has been carried out within the framework of the EUROfusion Consortium, funded by the European Union via the Euratom Research and Training Program (Grant Agreement No 101052200 − EUROfusion). In addition, this work has also been carried out within the framework of the Contract for the Operation of the JET Facilities and has received funding from the European Union's Horizon 2020 research and innovation programme. Views and opinions expressed are however those of the author(s) only and do not necessarily reflect those of the European Union or the European Commission. Neither the European Union nor the European Commission can be held responsible for them.

References

[1] Huber A *et al* 2018 *Nucl. Fusion* **58** 106021
[2] Silburn SA *et al* 2017 *Phys. Scr.* **T170** 014040
[3] Losada U *et al* 2020 *Nucl. Mat. Energy* **25** 100837
[4] De la Cal *et al* 2020 *Plasma Phys. and Controlled Fusion* **62** 035006
[5] Arnoux G *et al* 2014 *Phys. Scr.* **T159** 014009
[6] Eich T *et al* 2017 *Nuclear Materials and Energy* **12** 84-90
[7] Coenen J W *et al* 2017 *Physica Scripta*, **T170**, 014013
[8] Rack M *et al* 2014 *Nucl. Fusion* **54** 072004
[9] Huber A *et al* 2019 *Nuclear Materials and Energy* **18** 118-124
[10] Wiesen S *et al* 2017 Nucl. Fusion **57** 066024
[11] Figueiredo J *et al* 2016 *Rev. Sci. Instrum* **87** 11D443
[12] Joint European Torus - Wikipedia
[13] Huber V *et al* 2017 *Fusion Engineering and Design* **123** 979-985
[14] Gauthier E *et al* 2007 *Fusion Engineering and Design* **82** 1335-1340
[15] Balboa I *et al* 2012 *Rev. Sci. Instrum.* **83** 10D530
[16] Clever M *et al* 2013 *Fusion Engineering and Design* **88** no. 6-8 1342-1346
[17] Marot L *et al* 2015 *Journal of Coating Science and Technology* **2** 72-78
[18] Stamp M 2015 Technical Report No. UKAEA-CCFE-RE(23)01, UKAEA Culham Science Centre
[19] KP-M1AN/KP-M1AP datasheet, Hitachi Kokusai Electric Inc..
[20] Datasheet: https://www.kowaproducts.com/kowa-telephoto-lens/KowaTelephotoLensSpottingscope/
[21] Rose E, Stamp M 2016 Technical Report No. UKAEA-CCFE-RE(23)02, UKAEA Culham Science Centre
[22] Silburn S A 2022 Calcam version 2.8.3 doi: 10.5281/zenodo.6405602
[23] Stamp M 2015 Technical Report No. UKAEA-CCFE-RE(23)03, UKAEA Culham Science Centre
[24] Stamp M 2015 Technical Report No. UKAEA-CCFE-RE(23)23, UKAEA Culham Science Centre
[25] Last John 2014 Technical Report No. UKAEA-CCFE-RE(23)04, UKAEA Culham Science Centre
[26] A0M110 Aerotech Mounts: https://www.coherent.com.au/products/motion-control/optical-mounts/aerotech-aom-optical-mount-1286.html
[27] Durostone® EPC203 https://www.roechling.com/uk/industrial/materials/composites/epoxy-resin/durostone-epc-203
[28] Durostone® EPM03 https://www.roechling.com/uk/industrial/materials/composites/epoxy-resin/durostone-epm-203
[29] Durostone® EPRS1 https://www.matweb.com/search/datasheet.aspx?matguid=9d16409872a14522a154d33dd0097320&n=1&ckck=1
[30] Haist B *et al* 2009 *Fusion Eng. Des.* **84** 875-9
[31] Williams J C 2016 Technical Report No. UKAEA-CCFE-RE(23)05, UKAEA Culham Science Centre
[32] Williams J C 2015 Technical Report No. UKAEA-CCFE-RE(23)06, UKAEA Culham Science Centre
[33] De la Luna E *et al* 2016 *Nuclear Fusion* **56** 026001
[34] Fellowes D 2006 Kinematic and Quasi-Kinematic Constraints: What They Are & How
[35] Williams J C 2015 Technical Report No. UKAEA-CCFE-RE(23)07, UKAEA Culham Science Centre
[36] Lobel R 2014 Limb Stability e-mail communication
[37] Balboa I *et al* 2022 *Plasma Physics and Controlled Fusion*, submitted to this journal
[38] Naish J 2016 Technical Report No. UKAEA-CCFE-RE(23)08, UKAEA Culham Science Centre
[39] Fishpool G 2020 Technical Report No. UKAEA-CCFE-RE(23)12, UKAEA Culham Science Centre
[40] De Silva CW 2006 Vibration: Fundamentals and Practice Second Edition
[41] Williams J C 2020 Technical Report No. UKAEA-CCFE-RE(23)09, UKAEA Culham Science Centre
[42] Williams J C 2020 Technical Report No. UKAEA-CCFE-RE(23)10, UKAEA Culham Science Centre
[43] Williams J C 2020 Technical Report No. UKAEA-CCFE-RE(23)11, UKAEA Culham Science Centre
[44] Silburn S A 2021 Technical Report No. UKAEA-CCFE-RE(23)13, UKAEA Culham Science Centre
[45] Huber V *et al* 2016 *Rev. Sci. Instrum.* **87** 11D430
[46] Balboa I *et al* 2016 Rev. Sci. Instrum. **87** 11D419